The vacuum ultraviolet absorption spectra of norbornadiene. Vibrational analysis of the singlet and triplet valence states of norbornadiene by configuration interaction and density functional calculations.

Michael H. Palmer,[1,a] Søren Vrønning Hoffmann,[2,b] Nykola C. Jones[2,b] Marcello Coreno,[3,b] Monica de Simone,[4,b] Cesare Grazioli,[4,b] and R. Alan Aitken[5,b]

[1] *School of Chemistry, University of Edinburgh, Joseph Black Building, David Brewster Road, Edinburgh EH9 3FJ, Scotland, UK*

[2] *ISA, Department of Physics and Astronomy, Aarhus University, Ny Munkegade 120, DK-8000, Aarhus C, Denmark*

[3] *ISM-CNR, Instituto di Struttura della Materia, LD2 Unit 34149 Trieste, Italy,*

[4] *IOM-CNR Laboratorio TASC, Trieste, Italy*

[5] *School of Chemistry, University of St Andrews, North Haugh, St Andrews, Fife, KY16 9ST, Scotland, UK.*

[a)] Email: *m.h.palmer@ed.ac.uk*:

[b)] Electronic addresses: *vronning@phys.au.dk; nykj@phys.au.dk; marcello.coreno@elettra.eu; desimone@iom.cnr.it; grazioli@iom.cnr.it; raa@st-andrews.ac.uk*

ABSTRACT

A synchrotron-based vacuum ultraviolet absorption spectrum (VUV) of norbornadiene (NBD) is reported, and the extensive vibrational structure obtained has been analysed. The previously known $5b_1 3s$-Rydberg state has been reinterpreted by comparison with our recent high-resolution photoelectron spectral (PES) analysis of the X^2B_1 ionic state. Additional vibrational detail in the region of this Rydberg state is observed in its VUV spectrum, when compared with the PES $^2B_1$ ionic state; this is attributed to underlying valence state structure in the VUV. Valence and Rydberg state energies have been obtained by configuration interaction (CI) and time dependent density functional theoretical methods (TDDFT). Several low-lying singlet valence states, especially those which arise from $\pi\pi^*$ excitations, conventionally termed NV_1

to NV_4, have been examined in detail. Their Franck-Condon (FC) and Herzberg-Teller (HT) profiles have been investigated and fitted to the VUV spectrum. Estimates of the experimental 0^0 band positions have been made from these fits. The anomaly of observed UV absorption by the $^1A_2$ state of NBD is attributed to HT effects. Generally the HT components are less than 10% of the FC terms. The calculated $5b_13s$ lowest Rydberg state also shows a low level of HT components. The observed electron impact spectra of NBD have been analysed in detail in terms of triplet states.

I. INTRODUCTION

Recently, we reported synchrotron based, high-resolution photoelectron spectra (PES) for both norbornadiene (NBD) and quadricyclane (QC).[1] These isomeric compounds, shown in Figure 1, readily interconvert as discussed below, and this has led to numerous studies of the system having the potential for conversion of sunlight to electricity. We now present the previously unknown vacuum ultraviolet (VUV) spectra for NBD. The large amount of detail exposed, necessitates our corresponding study of QC to be delayed to a following paper. The PES for both compounds were previously analyzed in considerable detail by a combination of Møller-Plesset 4^{th} order perturbation theory, which included single, double and quadruple substitutions (MP4(SDQ)), configuration interaction (CI), multi-configuration self-consistent field (MCSCF) and density functional theoretical methods (DFT). Both are isoelectronic with cycloheptatriene (CHT) which we also studied recently, but lack conjugated double bonds.[2,3] Our theoretical approaches will be similar to those which were successful with CHT.

Interconversions between NBD and QC, and their derivatives are very important, since a promising approach to energy storage from the sun, lies in the use of strained organic molecules.[4-7] This justifies a brief summary. These so-called molecular solar thermal (MOST) binary systems, absorb solar energy via the alkene form (here NBD) leading to the strained

form (here QC); the stored energy can then be released from the latter catalytically, regenerating the NBD.

A related application for the NBD and QC system, is as a switch for an optical memory system.[8,9] The 'OFF' form of a photo-switch occurs when NBD, or one of its derivatives, are converted to the corresponding QC upon irradiation. Conversion back to NBD gives the 'ON' form of the switch. The stored energy is released as electricity, when the photo-switch interacts with a semiconducting electrode surface.

The NBD ⇆ QC interconversion occurs via an endothermic photoinduced [2+2] reversible cycloaddition.[10] The reverse reaction, where QC regenerates NBD with release of heat can occur via thermal or catalytic interaction, or even fluorescence.[7] When triplet sensitized using acetophenone, the NBD process appears to involve the two triplets, ^{3}NBD and ^{3}QC, followed by relaxation to QC,[10] but not all sensitizers behave similarly.[11] Since the nature of the triplet states involved in these processes are obscure; this has led us to include study the electron impact (EI) spectra of NBD. During the interconversion process, up to 100 kJ.mol^{-1} of chemical energy is stored, a value comparable to contemporary batteries.[12] Since the UV onset of NBD is 267 nm, a combination of donor and acceptor groups in the NBD+QC system is necessary to give an improved solar spectrum match, since the main wavelengths of sunlight lie between 300 and 700 nm. Examples have been reported with an onset of absorption up to 529 nm.[10,13,14] The UV-visible absorption spectra of substituted NBD and QC, show a strong blue shift when in the QC form.

NBD, isolated in argon, xenon or nitrogen matrices at 20K, gives quadricyclane when irradiated with UV light.[15] The selectivity of the photochemical reaction of NBD to QC has been rationalized in terms of matrix rigidity; this may exert a constraint on the transition state, where preference is given to the reaction where the product shape best fits the matrix site occupied by the reacting molecule.[16] The NBD ⇆ QC reaction is not exclusive in the gas

phase, since cyclopentadiene + acetylene, or even toluene can be formed.[15,17] All of these alternative products are thought to be formed by different C-C bonds breaking, and rearrangement of resulting diradicals.[15,17]

While technological aspects of the NBD ⇆ QC equilibrium lie outside the scope of the current paper, the electronically excited states for the parent molecules of NBD and QC are crucial to understanding these more complex interactions. Our theoretical work is directed to performing this at a more rigorous level than is currently available. However, the large amount of spectral study for NBD requiring our detailed analysis, makes it essential to deal with NBD first, and defer our parallel study of QC to a later paper. We do not discuss details of the dynamics of the NBD ⇆ QC process but refer interested readers to references 4 to 9 for recent discussions.

We analyze the VUV spectrum of NBD following the same procedures as with CHT and cyclooctatetraene[18,19] previously, in a detailed manner. We have determined both adiabatic and vertical excitation energies (AEE and VEE respectively), for singlet and triplet states of NBD. Where possible, we have retained C_{2v} symmetry, but for some states structural minimization led to saddle points rather than true minima; this led to relaxation of symmetry to C_1. The AEE methods used are mainly based on time-dependent density functional theory (TDDFT), a version of single excitation configuration interaction (CIS). VEE were determined by multi-reference multi-root singles and doubles configuration interaction calculations (MRD-CI); since these are performed at the X^1A_1 ground state structure, the results are VEE. Rydberg states are important, and these were treated theoretically through the use of very diffuse Gaussian-type basis functions.

The close proximity of the two (non-conjugated) double bonds in NBD leads to direct spatial overlap. This splits the degenerate isolated ethylenic moiety energy into symmetric (S) and antisymmetric (A) combinations for both π and π^* orbitals,[20-22] as discussed below. Much earlier literature on NBD used Mulliken's terminology of N(normal), V(valence upper state),

T(triplet) and R(Rydberg);[23] typical terms are NV for valence states. We combine this with more recent classifications involving the molecular orbitals (MOs) involved.[24]

Since NBD is an archetypal example of such through space interactions, there are a number of previous studies of its ultraviolet absorption (UV) spectrum,[25-30] as well as electron impact (EI)[31,32] and resonant multiphoton ionization (REMPI) spectra.[29,30] These have been critically reviewed by Robin.[16] Previous theoretical studies report analyses with varying levels of sophistication, which are integrated with our work below.

We report the UV+VUV absorption spectra and analyse these by high-level computational methods. Our interpretations are applied to each of the NBD absorption, EI and REMPI spectra. Much of our work has been devoted to adiabatic theoretical studies, enabling vibrational analyses by both Franck-Condon (FC) and Herzberg-Teller (HT) methods. Correlation of the theoretical envelopes with the experimental spectra allows identification of the 0^0 band origins, and hence AEE for the electronic states

Figure 1. The compounds norbornadiene (1a, NBD) and quadricyclane (1b, QC). The classical bond switching between the two systems occurs during UV excitation. For simplicity, H atoms are not marked for the cyclic moieties.

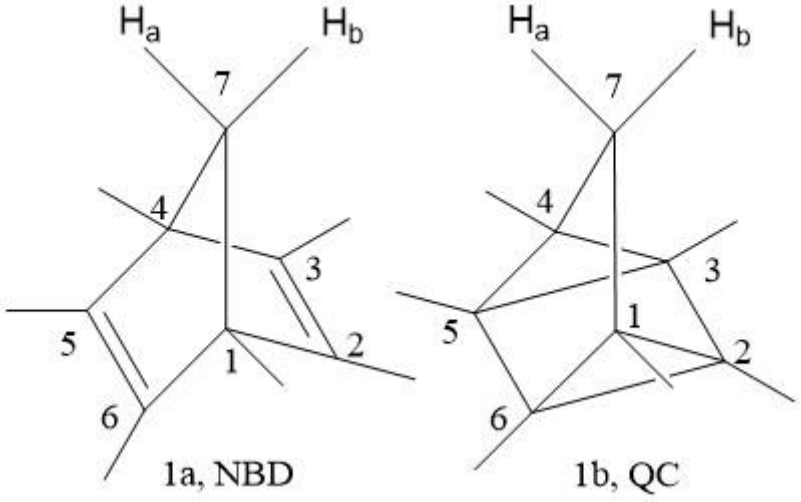

II. METHODS

The NBD sample, CAS registry number 121-46-0 and systematic name bicyclo[2.2.1]hepta-2,5-diene, was a commercial sample (ABRC, assay 99%) and used with no further purification.

A. The VUV absorption spectrum of NBD.

This was obtained at room temperature on the AU-UV beamline of the ASTRID2 synchrotron in Aarhus, Denmark, using methods described previously.[1,33] The overall photoabsorption spectrum is measured in small sections, in order that an appropriate pressure of sample gas can be chosen, depending on the local cross-section. For each region, an I_0 scan is first measured with the cell evacuated. The signal recorded from the photomultiplier tube (PMT) is a measure of the light intensity passing through the cell, with a measurement time of ~2 seconds per wavelength step. After filling the cell with the gaseous sample, two I_t scans of the attenuated light are measured. The cell is evacuated again and a second I_0 is measured; the process is repeated for each region of the spectrum measured. Using the number density (n) obtained through accurate measurement of the pressure, and the pathlength of the gas cell (l), the absolute photoabsorption cross-sections (σ) are then determined using the Beer-Lambert relationship:

$$I_t = I_0 \exp(-n\sigma l)$$

The full UV + VUV spectrum for NBD was covered by 3633 data points in the range 330 nm (3.857 eV) to 116 nm (10.751 eV). The data points are separated by 0.02 nm for most of the range, 0.1 nm up to 229.8 nm, and 1 nm from 280 nm to higher wavelengths.

The NBD spectrum, shown in Figure 2, exhibits fine structure in the 5.5 to 9 eV region superimposed on a series of broad peaks. One of these broad peaks is best seen by the logarithmic plot in SM1 as Figure SM1a.

Figure 2. Electron impact (EI) including electron-energy loss (EEL) spectra of Frueholz and Doering et el versus the present VUV spectrum for NBD. Several of the peaks above 6.5 eV are also present in the VUV spectrum, and hence are singlet states overlaying the current triplet ones. Conversely, the fine structure close to 8 eV in the VUV cannot be a Rydberg state.

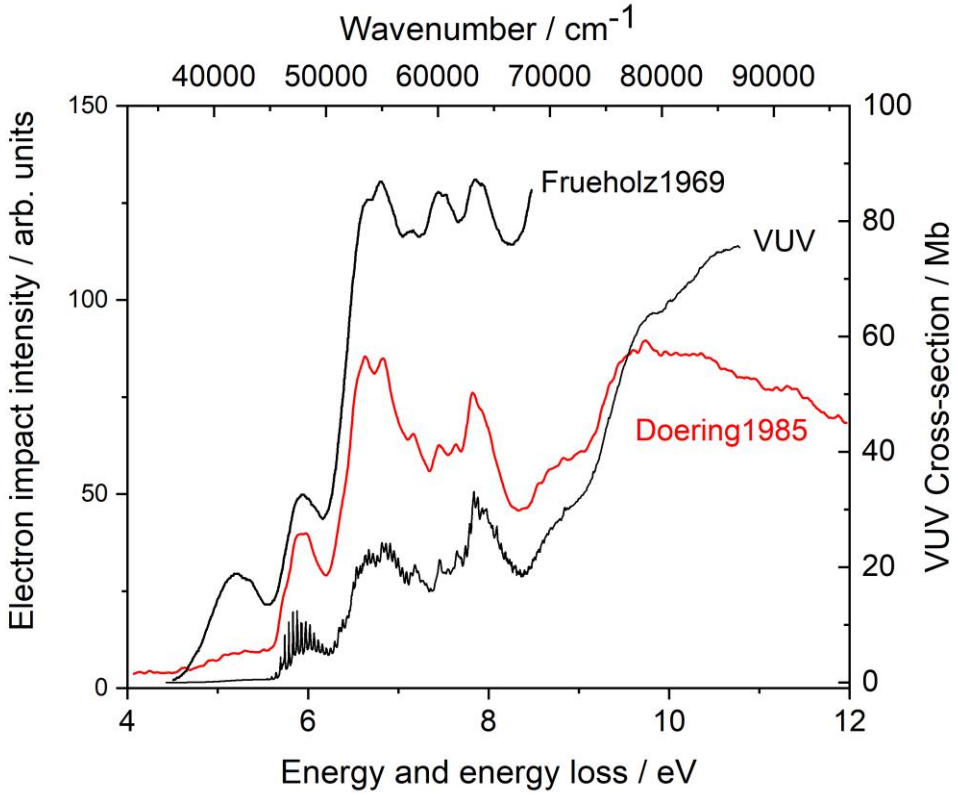

B. Theoretical methods.

As in our recent studies of NBD,[1] cycloheptatriene (CHT)[2,3] and cyclooctatetraene (COT),[18,19] we use several computational chemistry suites since no single suite can offer us a complete analysis. These include two Gaussian versions (G-09 and G-16),[34] as discussed further in the supplementary material under SM2. Vertical excitation energies (VEE) were determined by use of the MRD-CI method[35] in GAMESS-UK.[36] Vibrational features of the excited states, both FC and HT, were processed by the Pisa Group software,[37-39] as implemented in Gaussian. The equilibrium structures of both valence and Rydberg states were determined by time-dependent density functional theory (TDDFT).[40-42] The functionals used, included the Becke 3-parameter hybrid functionals (B3LYP)[43] and a long-range-corrected version of B3LYP, the Coulomb-attenuating method, CAM-B3LYP.[44]

The TDDFT suite in both G-09 and G-16[34] was used to determine the adiabatic excitation energies and their equilibrium structures for several valence states of each symmetry. It is necessary to correct these AEE to the energy difference at equilibrium between the X^1A_1 and excited state geometries, since both suites give the AEE as the energy difference at the excited state structure. This correction is performed automatically in both the FC and HT modules.

C. The principal basis sets.

Modern bases deliberately have a wide range of exponents, which can be used for both valence and Rydberg state determination. We have a clear distinction of purpose between these two types. Various older basis sets contain Gaussian type orbitals (GTOs) which are strictly valence in type; we used triple-zeta valence with single polarization (TZVP and 6-311G**).[45-48]

We calculate Rydberg states by adding very diffuse exponents to TZVP. These have exponents 0.021, 0.008 and 0.0026, positioned on C_7 as the unique atom, and have the same Gaussian exponents for s-, p-, d- and f-states.

III. RESULTS and DISCUSSION

Previous NBD experimental studies include UV-absorption,[25-30] EI,[31,32] REMPI[29,30] and circular dichroism(CD).[49] Several previous NBD theoretical studies have historical significance,[20-22,30,50-52] but do not contribute to the current level of understanding. Zgierski *et al*,[53] identified several theoretical criteria for interpretation of the NBD spectra, but were only able to pursue these aims using semi-empirical methods. McDiarmid and co-workers[29,30] contributed extensive spectroscopic studies of NBD, which were augmented by vertical excitation energy studies of some excitation processes for Rydberg states.

Our VUV absorption spectrum has a much larger energy range when compared with the REMPI study of the lowest Rydberg state by Xing et al.[29] Indeed, the spectral detail exposed in the present VUV is almost identical to the REMPI study, as shown in the supplementary material under SM3. Our recent PES study[1] of NBD showed much more vibrational detail than

earlier studies. Overlay of this new PES with its theoretical assignment, as in the supplementary material under SM4, onto our UV + VUV absorption spectrum, enables us to pinpoint the origins of several Rydberg states more precisely; this is performed below.

All orbitals and electrons are included in our computations; but we use valence shell numbering for occupied and virtual molecular orbitals (MOs and VMOs), to facilitate comparison with previous work. With the exception of a multiconfigurational second-order perturbation theory (CASPT2) study,[30] most previous discussion of the valence MOs has been in a solely π-electron context, although mixing with the σ-MOs was understood.[20-22] In the current C_{2V} coordinate system, the NBD valence shell is: $7a_1+5b_1+4b_2+2a_2$ with core MOs: $3a_1+1b_1+2b_2+1a_2$. In studies where alternative NBD C_{2V} coordinate axes are used, interchanges of both b_1/b_2 MOs and B_1/B_2 states occur.

The degenerate π-MOs and their antibonding conjugates, form symmetric (S) and anti-symmetric (A) combinations; these were conventionally termed as normal valence (NV_1 to NV_4) in Mulliken's notation,[23] or SS (a_1), AS (b_1), A*S* (b_2), A*A*(a_2) in Hoffmann's terms.[22] In practice, the mixing of π- and σ-atomic orbitals is very apparent, as is shown in supplementary material as SM5.

The ground state NBD molecular structure has been determined by both electron diffraction[54] and microwave Fourier transform spectroscopy.[55] Our X^1A_1 structures for all bases used, are very similar, but since structural results for several singlet and triplet valence states of NBD are not central to this theoretical analysis, they are shown in the supplementary material as SM6.

1. The NBD theoretical singlet and triplet state manifolds.

The principal triplet and singlet state equilibrium structure results are shown in Tables I and II. Excitation energies are corrected to be differences between ground and excited state energy,

where both are at their respective equilibrium structures; this follows standard spectroscopic practice.

The highest occupied molecular orbital (HOMO) and lowest virtual orbital (LUMO) sequence numbers, 26 and 27 in the Aufbau energy sequence, apply irrespective of symmetry changes. We note that two pairs of MOs: $4b_2$ and $2a_2$ and $6b_2$* and $6b_1$*, are nearly degenerate, but in general, we express our discussion in terms of states and their energies; the constituent MOs only occur when denoting the composition of configurations.

Using the TDDFT method with the 6-311G** basis set, we find 13 singlet state vertical excitation energies (VEE) below 8.0 eV. Our state binding energies in C_{2v} are shown in Figure 3. Where linear combinations of configurations are shown, both eigenvectors are greater than ±0.1, with the largest value first. The adiabatic excitation energies, all lie lower in energy, a result of structural relaxation, but by variable amounts, as is discussed below.

Strictly, the ππ* excitations, as originally defined,[22,23] involve promotions from doubly occupied MOs 24 ($7a_1$) and 25($5b_1$) to 26 ($5b_2$*) and 27($3a_2$*), leading to NVn with n=1 to 4. However for NBD, mixing of the local π or π* with σ or σ* AOs occurs, leading to additional complexity, as demonstrated in the supplementary material as Figure SM5. Simple combinations of A*S* and S*S* do not occur; this was first appreciated by Zgierski and Zerbetto,[53] in their (semi-empirical) spectroscopic parameterized complete neglect of differential overlap method (CNDO/S) study. They proposed major structural changes occurred between the ground state (S_0) and the lowest two singlet states (S_1 and S_2), but we do not concur with that view, as discussed in the supplementary material as SM7.

Figure 3. The lowest set of singlet state vertical excitation energies, using the TDDFT method with a triple zeta basis set. Where more than one leading term is shown, both eigenvectors are greater than ± 0.1, with the configuration with largest value first. Where two states are nearly degenerate, as in $^1A_1$+$^1B_2$, and $^1A_2$ + $^1B_1$, all close to 7 eV, the energy level is thickened. In some cases, such as the two $^1A_1$ states at 6.96 and 7.84 eV, the nature of the two states is very different; these are $5b_16b_1$* and $4b_25b_2$* respectively.

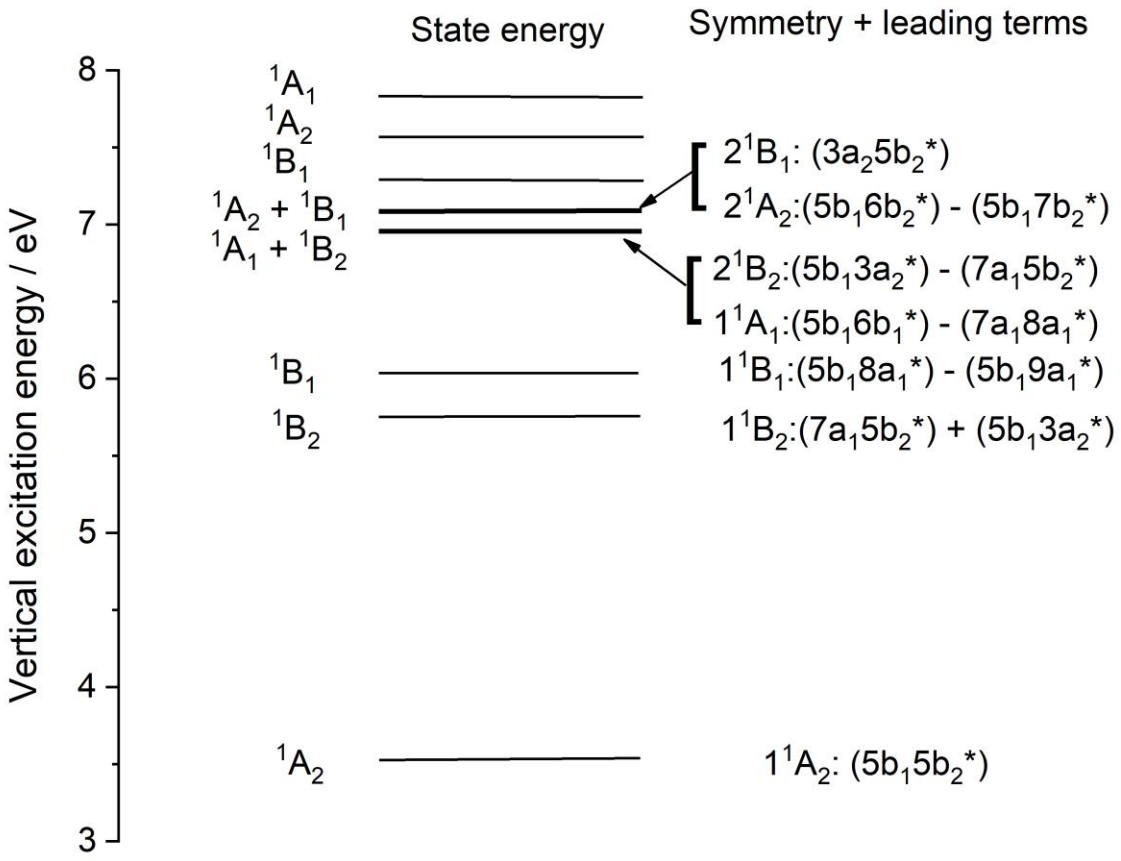

2. The electron impact spectral onset for NBD.

These have been obtained for NBD by Doering and McDiarmid,[28,29] Frueholz et al[31] and Allan,[32] and occur in the 2.8 to 5.5 eV range**.** The profiles of EI spectra vary considerably with change in the impact electron energy and scattering angle; these are discussed further in the supplementary material as SM8.[28,31,32] A comparison of two of these EI spectra with the VUV spectrum is shown in Figure 2. Considerable differences in the relative peak intensities are exhibited in the two EI methods and the VUV spectrum.

The presence of a strong peak in all the spectra shown in Figure 2, is indicative of a valence state. The one close to 8.0 eV must be the highest of the ππ*-states, NV_4. Variations in the EI intensity with scattering angle for the 5.23 and 7.5 eV peaks, suggest that these are forbidden relative to the 5.95 and 6.65 eV peaks. Doering and McDiarmid[28] summarized the observed electron impact ππ* VEE as: $^1A_2$ (5.25, $b_1b_2^*$), $^1B_2$ (5.95, $a_1b_2^*$), $^1B_1$ (6.65, $b_1a_2^*$) and $^1A_2$

(7.5eV, a_1a_2*); those at 5.95 and 6.65 eV overlap with 3s- and 3p-Rydberg states respectively. These proposals, based on variations in intensity with high and low incident energies, have been widely accepted.

Our vertical excitation (VEE) triplet state energy results were determined using the MRD-CI method[35] in GAMESS-UK;[36] all single and double substitutions from the ground state wave-function (at equilibrium) are included. The calculated triplet state VEE in Table I, are relatively close to Allan's spectral maxima,[32] and are displayed in Figure 4. These were obtained using a strictly valence TZVP basis set, so no Rydberg state participation can occur through these calculations. Table I also shows the single excitation TDDFT results for the VEE determined at the X^1A_1 structure. Although the two lowest triplet state energies are close between the two methods, there is considerable scatter for the higher values when comparing similar states of same symmetry. However, the overall correlation has a slope of 1.032 (where the MRD-CI values (x) are lower, and the line apparently goes through the origin, since the intercept is smaller than its standard deviation. Since the MRD-CI values use a higher level of correlation than TDDFT, we regard those values as more realistic.

The lowest electronically excited triplet state (T_1), is the HOMO → LUMO process, generating the $^3A_2$ state (largely $5b_15b_2$*). This has calculated AEE (using the TDDFT method) and VEE (MRD-CI) of 2.189 and 3.056 eV. These are significantly lower values than the apparent EI onset of 3.47 eV, and maximum 3.88 eV respectively.[32] Experimentally, T_1 only appears as a shoulder on the leading edge (lower energy) side of the second triplet state (T_2). The combined T_1+T_2 unit, shown in Figure 4, covers the energy range 2.9 to 4.5 eV.[31] Allan suggests that the $^3B_2$ state (T_2) has onset is at 3.76 eV, but the present AEE and VEE are again significantly lower at 3.029 and 3.386 eV respectively. T_2 shows vibrational structure[32] with apparent frequency 1210 cm^{-1} which is close to an a_1 mode which we calculate at 1170 cm^{-1} for the $^3B_2$ state. The present symmetry sequence of T_1 and T_2 are in agreement with the previous VEE

study.[30] The a_1 frequencies for the $^3A_2$ and $^3B_2$ states are shown in the supplementary material section SM9.

Table I. Triplet state vertical excitation energies (VEE) using the MRD-CI and TDDFT methods. The leading configurations have valence shell numbering, with eigenvectors showing the proportions where there are two leading terms. The TDDFT determinations were at the X^1A_1 equilibrium structure. The correlation between the two determinations is: VEE_{TDDFT}= 1.032(117)*VEE_{MRDCI} +0.690(782), where the standard deviations for slope and intercept are in parentheses; the correlation coefficient, adjacent R-square, is 0.818.

MRD-CI			TDDFT
VEE / eV	Symmetry	Leading configurations	VEE / eV
3.056	$^3A_2$	0.891 ($5b_15b_2$*) - 0.210($7a_13a_2$*)	3.264
3.386	$^3B_2$	0.701 ($7a_15b_2$*) - 0.517 ($5b_13a_2$*)	3.711
5.122	$^3A_1$	0.903 ($5b_17b_1$*) - 0.193 ($7a_18a_1$*)	7.573
5.909	$^3B_1$	0.920($5b_18a_1$*)	7.149
6.081	$^3A_1$	0.915 ($5b_16b_1$*)	7.691
6.556	$^3B_2$	0.591 ($7a_15b_2$*) + 0.671 ($5b_13a_2$*)	6.100
6.559	$^3A_2$	0.895($4b_15b_2$*) – 0.163($7a_13a_2$*)	6.814
6.585	$^3A_1$	0.806 ($5b_17b_1$*) + 0.441($7a_18a_1$*)	8.222
6.756	$^3B_1$	0.896 ($5b_111a_1$*)	7.213
6.841	$^3A_2$	0.541($7a_13a_2$*) - 0.215($5b_16b_2$*)	8.010
6.957	$^3B_2$	0.861($5b_14a_2$*) + 0.262($7a_16b_2$*)	8.282
7.122	$^3A_2$	0.202($7a_13a_2$*) + 0.625($5b_16b_2$*)	8.166
7.244	$^3A_1$	0.818 ($7a_18a_1$*) + 0.426($5b_17b_1$*)	8.234
7.625	$^3B_1$	0.896($5b_110a_1$*)	7.934
7.698	$^3B_1$	0.896($5b_19a_1$*)	8.523
7.784	$^3B_2$	0.854($7a_16b_2$*) + 0.337($5b_14a_2$*)	8.941
7.966	$^3B_1$	0.913 ($7a_17b_1$*)	8.904
8.058	$^3A_2$	0.817($5b_17b_2$*)	8.729

Table II. Adiabatic excitation energies (AEE) and oscillator strengths for singlet states using the CAM-B3LYP functional at the TDDFT level. Comparison with the MRD-CI VEE method, which includes single and double substitutions in the reference configurations. AEE corrections to the TDDFT AEE are included, as described in supplementary material SM10. The leading term is shown first, and the orbitals use valence shell numbering. The linear correlation between the two determinations is: AEE_{TDDFT}= 1.070(192)*VEE_{MRDCI} – 1.516 (1510), where the standard deviations for slope and intercept are in parentheses. The correlation coefficient, adjacent R-square, is low at 0.750. The VEE correlation between TDDFT and MRD-CI over the tabulated values is poor; adjacent R-square is 0.684 and slope 0.68(13). An extended list of the TDDFT singlet states is shown in the supplementary material as

TDDFT						MRD-CI	EI[32]	Roos et al[30]	
State	Root	Leading configurations	Corrected AEE / eV	Oscillator strength f(r)	VEE /eV	VEE / eV	VEE / eV	CASSCF /eV	PT2 / eV
1^1A_2	NV_1	$5b_15b_2$*	3.996	0.0	3.545	5.818	5.23,5.25	8.18	5.28

1^1B_2	NV_2	$7a_15b_2^* + 5b_13a_2^*$	5.762	0.0246	5.756	6.854	5.92, 5.95	9.42	6.20
2^1A_2	NV_3	$7a_13a_2^*+5b_15b_2^*$	6.216	0.0	7.095	7.795	6.65	9.78	6.48
1^1B_1		$5b_18a_1^*- 5b_19a_1^*$	6.856	0.0098	6.036	7.541			
1^1A_1		$4b_25b_2^*$	6.899	0.0122	6.954	7.244			
2^1B_2	NV_4	$5b_13a_2^*+7a_15b_2^*$	6.901	0.2005	6.960	7.756	7.50	10.40	7.36
2^1B_1		$2a_25b_2^*-5b_18a_1^*$	7.272	0.0243	7.133	8.456			
2^1A_1		$5b_16b_1^* + 7a_19a_1^*$	7.582	0.0021	7.841	7.588		7.97	7.49
3^1B_1		$5b_18a_1^*+2a_25b_2^*$	7.782	0.0011	7.291	8.950			
3^1B_2		$6a_15b_2^*$	7.853	0.0025	7.942	9.068			
3^1A_2		$5b_15b_2^*+7a_13a_2^*$	7.929	0.0	7.973	8.499			

Figure 4. Assignment of Allan's triplet state manifold[32] using vertical excitation energies calculated by the MRD-CI method.

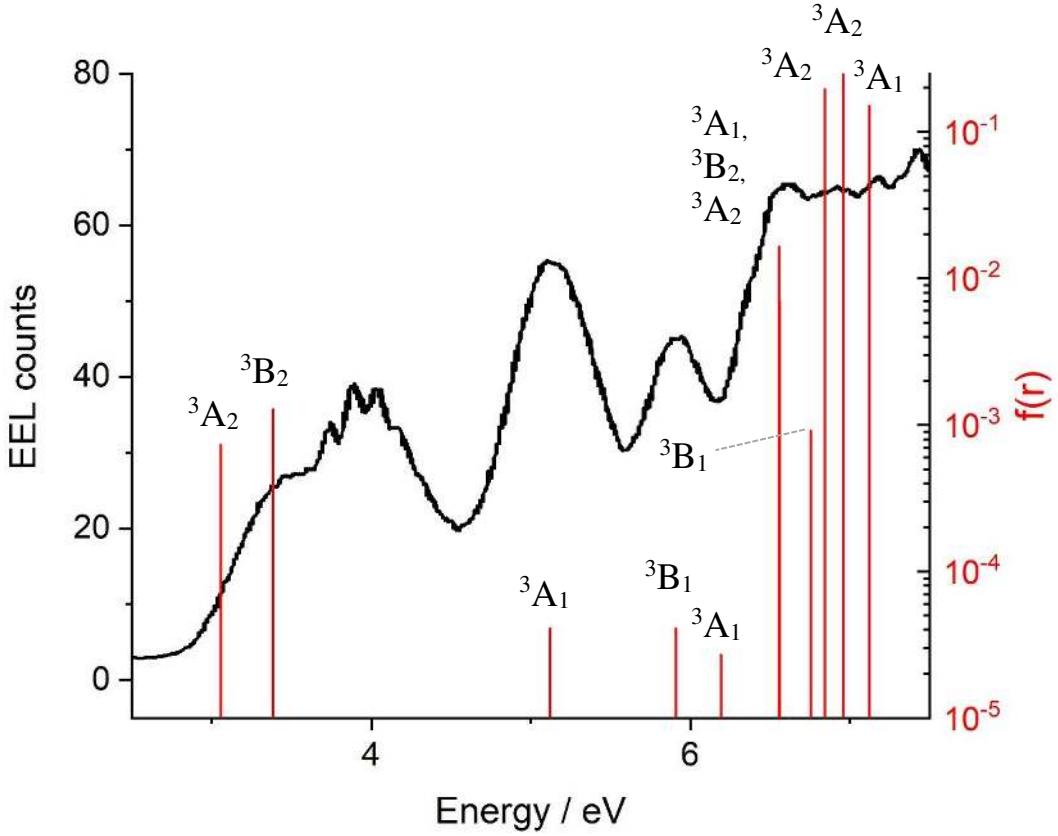

The energy region near 5.1 eV in Figure 4, corresponds to the $^3A_1$ state (T_3) calculated energy at 5.122 eV, but this region also contains the lowest singlet state, the $^1A_2$ (NV_1) state, as discussed below. The two states calculated at 5.909 ($^3B_1$, $5b_18a_1^*$) and 6.081 eV ($^3A_1$, $5b_16b_1^*$) are assigned to the EI peak at 6.0 eV. The EI region above 6.5 eV, shown in Figures 2 and 4, is crowded by calculated triplet states. The peak at 7.873 eV both in the VUV, and the Doering[25] and Frueholz[31] EI studies, is not present in the Allan study,[32] and hence must be a valence state; this is discussed further below. It is important to recognize that the theoretical basis set used here, is purely valence in character, and hence cannot generate Rydberg states.

3. The onset of optical absorption for NBD.

The EI spectra display two well defined broad peaks at 5.25 and 5.95 eV, which are best seen in the Frueholz et al spectrum.[31] These have been assigned as $^1A_2$ (b_1b_2*) and $^1B_2$, (a_1b_2*) respectively. The onset of the optical spectrum, shows only a shoulder at 5.4 eV.[25-30] This shoulder has been attributed to the lowest ππ* singlet excitation (NV_1) of norbornadiene**.** The work of Robin and Kuebler studying NBD at various temperatures, established the 0-0 band as 5.608 eV(45230 cm^{-1}).[26] Lightner et al,[50] using circular dichroism, also observed this state in ethanol solution, as a shoulder at 5.391 eV (230 nm). Its presence in solution indicates a singlet valence state.[24,50] The adiabatic ionization energy (AIE_1) for NBD is 8.279 eV.[1] The present band with origin 5.608 eV, is separated from this by 2.671 eV, which is not suitable for a 3s-Rydberg state.

The NV_1 state symmetry, first established by Zgierski and Zerbetto[53] as the $^1A_2$ state, was calculated at 5.982 eV (208 nm); this was an important, but fortuitous advance in 1993, since such CI energies were very dependent upon the empirical parameters used. Their analysis,[53] part of a study on the ground, first and second excited states (S_0, S_1 and S_2) of NBD, concluded that major structural changes occurred for both excited states. This included lengthening of the C-H bonds, and closing of the $C_2C_1C_6$ angle between the two local planes containing the double bonds ('wings'). This angle, and also one dihedral angle, are incorrectly labelled[53] as $C_4C_3C_5$, but are unambiguous from their citation with structural data.[54]

We have computed the equilibrium structures for all three states, using the CAM-B3LYP method under TDDFT conditions, We agree that the $C_2C_1C_6$ angle is considerably different in the X^1A_1 state (107.1°) from that in the $^1A_2$ state (88.2°); however, the C-H bond lengths and CCH angles differ in trivial amounts between the two states. The structural bond length changes involving the H-atoms, claimed[53] to be 0.37Å, must be an artefact of their calculations. Details of the structures are given in the supplementary material under SM6 and SM7.

Similarly, in order to determine the vibrational contributions to these electronic states, we sought the AEE using the TDDFT method with the CAM-B3LYP functional and the TZVP basis set. Since details of these calculations are not central to the current theme, they are shown in Table II, but discussed in the supplementary material as SM10.

Although the lowest singlet state of NBD is generally agreed to be the 1^1A_2 state, this is optically forbidden under Franck-Condon rules.[20-22,30,50-52] This dilemma is resolved by the presence of non-symmetric vibrations, which are allowed under Herzberg-Teller (HT) rules as shown below.

4. The Herzberg-Teller (HT) profile of the 1^1A_2 state.

Since the theoretical behaviour of this 1^1A_2 state is typical of HT states, it is treated in more detail than some succeeding states. The standard convention for vibrational mode sequence for NBD in C_{2V} symmetry is a_1: 1 to 12, a_2: 13 to 20, b_1: 21 to 29, b_2: 30 to 39. Whilst we adhere to this convention, we note that the most prominent modes are those of lowest frequency, and hence highest sequence numbers. So we retain both systems, noting that when 'mode' is used we refer to standard usage; in contrast, 'sequence number', refers to the ascending frequency sequence. All such results in G-09 and G-16 use this convention. Full sets of harmonic frequencies and the G-09/G-16 labelling system for the lower excited states, are in the supplementary material at SM11. In this and all following Sections, FC and/or HT intensities are given as molar absorption coefficient ($dm^3.mol^{-1}.cm^{-1}$). The 'position' is relative energy from the 0-0 (0^0) calculated band.

The HT analysis for NV_1, shows that several sequences of binary and tertiary combination bands occur; these have maximum intensity distant from the generally low intensity of the 0-0 position. One series containing combinations of modes 12 ($12a_1$, 368 cm^{-1}) and 39 ($10b_2$, 306 cm^{-1}) has its maximum with the 10^{th} member at 4465 cm^{-1} from 0-0. The most intense bands of the HT profile, shown in Table III, consists of several non-symmetric vibrations combined

with a $12a_1^n$ carrier, where *n* is the number of quanta; generally *n* is greater than 10 for significant intensity to occur, while the maximum intensity occurs for *n* = 18. Other vibrations, having minor intensity in Table III, also involve a_1 modes as carriers. Since both the HT (and FC) vibrational states generate a large number of vibrational states; we have limited the Tables to combinations of two simultaneously excited modes, while all states are included in Figure 6. HT bands are generally relatively weak in comparison with FC bands.

The vibrational contributions giving the most intense binary combination series are: $12^9 39^1$ through to $12^{30}39^1$ with maximum intensity at $12^{19}39^1$. The most intense HT band overall, combines these with mode 5 (a_1, 1431 cm^{-1}). This corresponding triple combination series has maximum intensity for $5^1 12^{19} 39^1$. In addition to modes 12, 39 and 5, shown in Table III, other binary modes participating in the HT calculations for the $^1A_2$ state, in conjunction with 12^n, are: 10^1, 10^3, 10^5, 10^7 (all b_2), 19^1, 18^1,17^1 (all a_2), 38^1, 38^3, 37^1, 34^1, 33^1(all b_2), 28^1, 26^1, 25^1, 24^1, 23^1 (all b_1), where the quanta are given in superscripts.

The UV absorption, shown in Figure 2, shows a clearly sigmoidal rise of signal strength towards the onset of the 5.95 eV Rydberg state sequence (as discussed below), and there is an overlap of the vibrations for the HT band with the following Rydberg state. The present HT calculations suggest that absorption starts significantly below 4.5 eV. The calculated origin for the 0-0 transition is 3.873 eV (31241cm^{-1}). As expected for a formally forbidden transition, the 1^1A_2 (S_1) state shows no Franck-Condon vibrational bands. The extensive HT vibrational profile obtained is exemplified in Figure 6. In order to correlate the observed sigmoidal rise of the experimental spectrum with the calculated HT profile, we have increased the calculated HT energies by 0.335 eV to fit the electron impact maximum at 5.23 eV.

Not all of the bands involve combinations of a_1+b_2 vibrations. Various combinations of HT bands occur, mainly from the low and mid-frequency fundamentals. The high frequency C-H stretching modes are absent. Since all calculations of the S_1 state ($^1A_2$) are carried out

independently from those for the S_2 ($^1B_2$) and S_4 ($^1B_1$) states below, there is no possibility of b_2 modes inducing intensity in S_1 by stealing from either the S_0 to S_2 or S_0 to S_4 transitions. Thus it is not essential to postulate the stealing proposed by Zgierski et al, when considered in the HT as opposed to FC context.[53] Further, all of the modes showing HT activity above for the $^1A_2$ state, have significantly lower frequencies than the 1600 cm^{-1}, C=C (b_2 stretching vibration) previously thought[53] to be prominent in the intensity of S_1.

Figure 5. The onset of absorption for NBD following Frueholz et al, in the region 4.0 to 6.5 eV region; the electron energy-loss spectrum is at a scattering angle of 20° and 50 eV incident energy. The Herzberg-Teller (HT) profile is superimposed with vibrational bands having Half-Width at Half-Maximum of 10 (red) ,70 (blue) and 400 cm^{-1}(magenta). All band widths are expressed as HWHM, but with varying widths. The intensity of the HT peak is scaled by a factor of two relative to Table III.

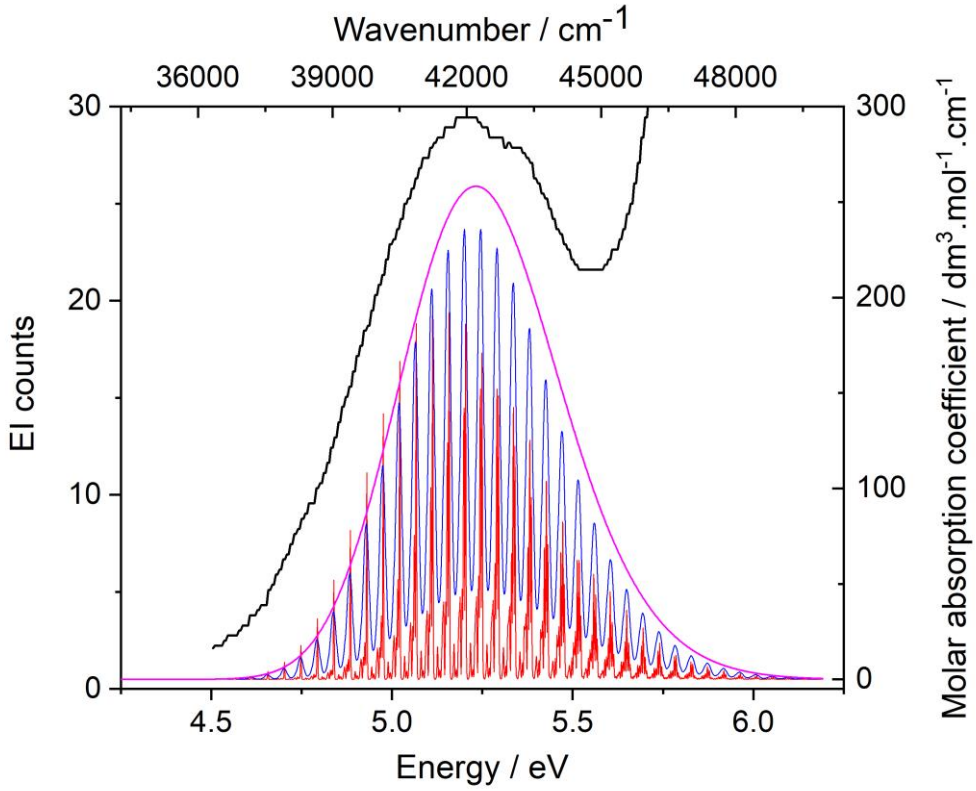

Table III. The most intense 1^1A_2 state Herzberg-Teller modes determined using the CAM-B3LYP functional in the TDDFT method. The complete envelope contains 880 vibrational states for binary and tertiary combinations; an extended list is shown in the supplementary material as SM8. The terminology: 12^16;39^1 refers to a binary combination mode, where 16 quanta of sequence mode 12, is combined with 1 quantum of mode 39; in conventional terms this is mode $12^{16}+39^1$.

Mode	Position /cm^{-1}	Intensity
12^16;39^1	6191	86

12^17;39^1	6558	101
12^18;39^1	6926	112
12^19;39^1	7294	115
12^20;39^1	7662	110
12^21;39^1	8030	99
12^22;39^1	8397	84
5^1;12^16;39^1	7621	95
5^1;12^17;39^1	7989	111
5^1;12^18;39^1	8357	121
5^1;12^19;39^1	8725	123
5^1;12^20;39^1	9092	117
5^1;12^21;39^1	9460	104
5^1;12^22;39^1	9828	87

5. The NV_2 valence state: the 4.5 to 6.5 eV range.

The sigmoid rise in absorption here carries a set of sharp bands on top of rising intensity. This indicates the presence of at least two states in this region. Zgierski et al[53] denied the presence of a Rydberg state in their CNDO/S study of the 5.827 eV (47000 cm^{-1}) region, and claimed that it contained only a $^1B_2$ valence state; however, the nature of their calculations would not have detected a Rydberg state. This becomes important below, since their $^1B_2$ valence state frequencies were later used in the REMPI study of a Rydberg state by Xing et al.[29] Doering and McDiarmid[28] suggest that the NV_2 ($^1B_2$) valence state is the EI peak at 5.95 eV. This valence state was observed by Robin,[27] in the presence of a high pressure of helium gas, which selectively reduces the cross-section of the Rydberg state.[27] In summary, a number of UV+VUV absorption, REMPI and theoretical calculations have all agreed that this NV_2 valence state has a Rydberg state superimposed.[20-22,29,30,50-52]

Robin et al's high pressure VUV absorption spectrum[27] is combined with both the EI spectrum of Frueholz et al, and the present Franck-Condon profile in Figure 6. Although the intensities of the FC profile shown differ from experiment considerably, the principal local maxima from the experiment are close to the red set of calculated peaks, which have Half-Widths at Half-Maximum (HWHM) of 10 cm^{-1}; this represents a close correlation which enables assignment of the 0-0 band from the calculated value. There is generally good agreement between the FC

profile and the high pressure VUV spectrum, and this appears to establish the NV_2 state origin as 5.730 eV for the $^1B_2$ state.

Figure 6 shows that there is considerable intensity in the 0-0 band. Several of the prominent modes excited under Franck-Condon conditions, and given in Table IV, show that all a_1 modes except mode 1 contribute to the profile.

The mode 12^n sequence where n is the number of quanta, has an unexpected dip in the intensity of the n=3 member, compared with those with n= 2 and 4. We note that mode 11 is almost exactly double the frequency of mode 12. As a consequence 12^3 is almost degenerate with the binary combination 11^112^1; both have much lower intensities than other members of their sequences. Other accidental near-degeneracies at the harmonic level are mode 9 with modes 11 + 12, and mode 7 with modes 10 + 11. Some of these near-degenerate levels can be expected to show significant interactions in anharmonic calculations, but these were not pursued further in this work. Among the more intense binary combinations are 12^n20^2, an a_2^2 series, and a_1 combinations 11^112^n, 10^112^n and 7^112^n.

Figure 6. The NV_2 band (blue) exposed from the VUV spectrum by 136 atm of helium gas and from the electron impact spectrum (black) at a scattering angle of 20° and 50 eV incident energy. The calculated Franck-Condon profile with energy scale increased by 0.1288 eV is superimposed in red. The 0-0 band is at 5.731 eV (46206 cm^{-1}).

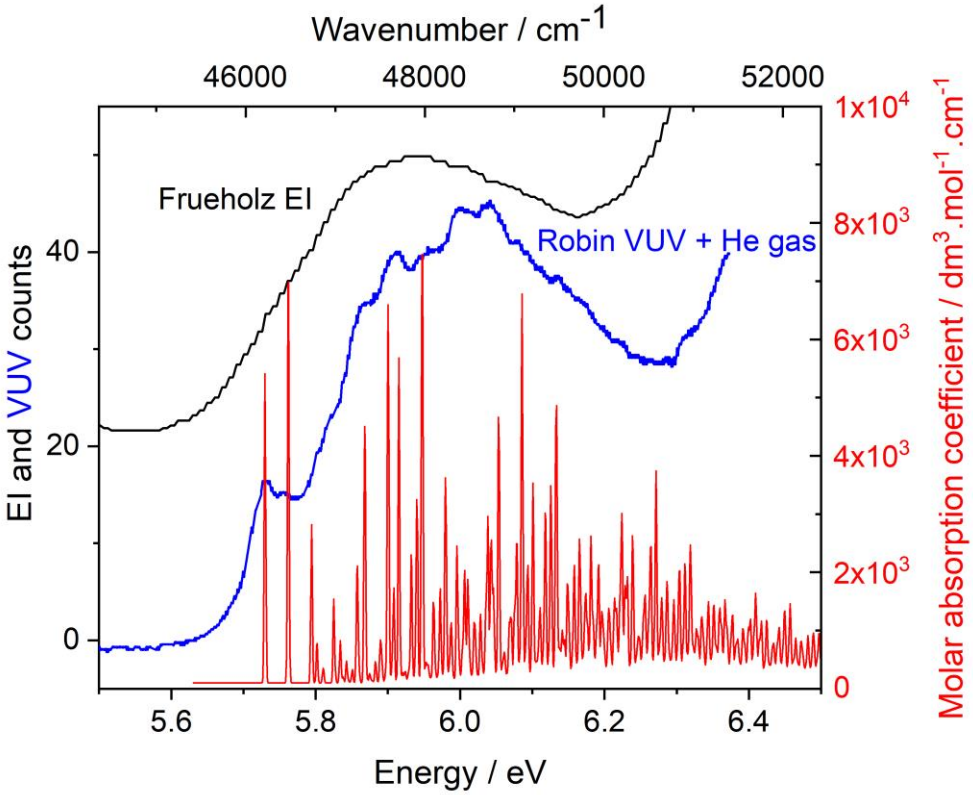

Table IV. The most intense 1^1B_2 state Franck-Condon modes determined using the CAM-B3LYP method. The complete envelope contains 880 vibrational states from binary through to quintet combinations. The most intense band: 29^1;1^1 refers to a binary combination, where 1 quantum of sequence mode 29, is combined with 1 quantum of mode 1, from Table V; in conventional terms this is mode 29^1+1^1. The position is relative energy from the 0-0 calculated band; intensity is the molar absorption coefficient ($dm^3.mol^{-1}.cm^{-1}$) throughout the text and tables of this study.

Mode	Position /cm^{-1}	Intensity
1^1	260	6871
1^2	520	2745
21^1	1115	4385
21^1;1^1	1375	4718
29^1	1496	3609
28^1;1^1	1699	2451
29^1;1^1	1756	7287
21^2;1^1	2490	2626
29^1;21^1	2611	4239
29^1;21^1;1^1	2871	4755
29^1;1^1	3131	2234
29^1;28^1;1^1	3194	2402
29^2;1^1	3252	3598
29^1;21^2;1^1	3985	2430

Table V. The most intense 1^1B_2 state Herzberg-Teller modes determined using the CAM-B3LYP method. The most intense band: 29^1;1^1 refers to a binary combination, where 1 quantum of sequence mode 29, is combined with 1 quantum of mode 1, from Table V;

in conventional terms this is mode 29^1+1^1. The position is relative energy from the 0-0 calculated band; intensity is the molar absorption coefficient ($dm^3.mol^{-1}.cm^{-1}$) throughout the text and tables of this study. The complete envelope contains 1232 vibrational states for binary through to quintet combinations.

Mode	Position /cm^{-1}	Intensity	Symmetry
2^1	325	18	A_2
3^1	465	2	B_2
7^1	546	4	A_2
2^1;1^1	586	29	B_1
9^1	679	19	B_2
10^1	705	1	A_2
9^1;1^1	941	34	B_2
2^3	975	2	A_2
19^1	1049	36	A_2
17^1;1^1	1258	23	B_2
19^1;1^1	1310	41	A_2
24^1;1^1	1505	24	A_2
19^1;1^2	1571	17	A_2
21^1;2^1;1^1	1701	22	A_2
21^1;9^1	1794	23	B_2
29^1;2^1	1821	18	A_2
21^1;9^1;1^1	2055	23	B_2
29^1;2^1;1^1	2082	31	A_2
21^1;19^1	2163	29	A_2
29^1;9^1	2175	19	B_2
21^1;19^1;1^1	2425	44	B_1
29^1;9^1;1^1	2436	36	B_2
29^1;19^1	2544	37	A_2
24^1;21^1;1^1	2620	19	A_2
29^1;17^1;1^1	2754	25	B_2
29^1;19^1;1^1	2805	44	B_1
29^1;24^1;1^1	3001	26	A_2

6. The $^1B_1$ 3s-Rydberg state and its vibrational properties: the 4.5 to 6.5 eV range.

The most detailed previous study of the Rydberg state is the resonant-enhanced multiphoton ionization ((2+1) REMPI) of Xing et al,[29] with additional features shown by Roos et al.[30] Both UV-absorption and two REMPI studies led to assignment of the series of bands between 5.4 and 6.2 eV as the $5b_1$3s-Rydberg state; these conclusions preceded our high-resolution PES study, and were based on the largely unresolved broad PES band known at the time, a successful prediction. A comparison of the VUV absorption spectral results of this state with the X^2B_1 ionic state profile is shown in Figure 7.

Figure 7. Superposition of the experimental photoelectron spectrum (in red), shifted by 2.8374 eV to lower energy, and the VUV state (in blue) in the 5.5 and 6.5 eV region. It is clear that the VUV region contains a number of weak peaks which are not present in the ionic state; these indicate the presence of an underlying valence state.

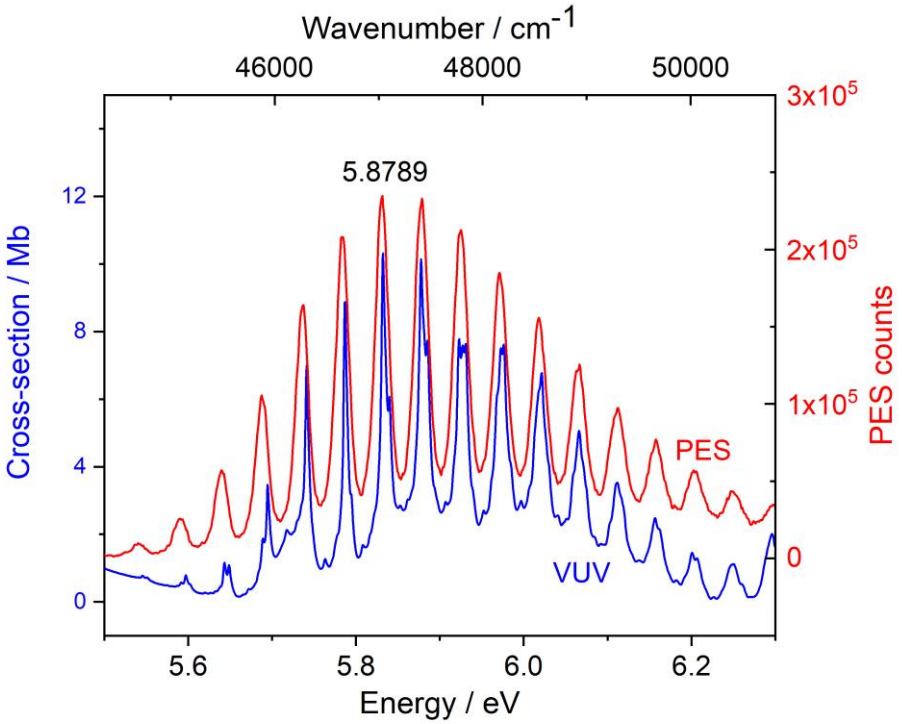

The experimental PES X^2B_1 ionic state (in red), can be superimposed upon the 5.5 to 6.5 eV of the VUV spectral region (in blue), as shown in Figure 7, by a shift of 2.837 eV to lower energy. Application of the Rydberg energy equation, leads to a value of $n - \delta = 2.199$; this implies the principal quantum number $n = 3$ with quantum defect $\delta = 0.801$. The previously reported[1] individual calculated vibrational FC peaks, with a narrow (10 cm^{-1}) linewidth, generally offer both a good interpretation of the apparent underlying broad region below the Rydberg state as seen in Figure 8. Some very weak peaks lying below the Rydberg state, which do not occur in either the ionic state itself, or the theoretical profile which describes it, can be attributed to underlying valence state structure.

Figure 8. Comparison of the VUV spectrum of the 3s-Rydberg state ($^1B_1$) of NBD (in black) with the hot band structure for the X^2B_1 state (in red). The half-width at half-maximum (HWHM) of the theoretical study is 10 cm^{-1}.

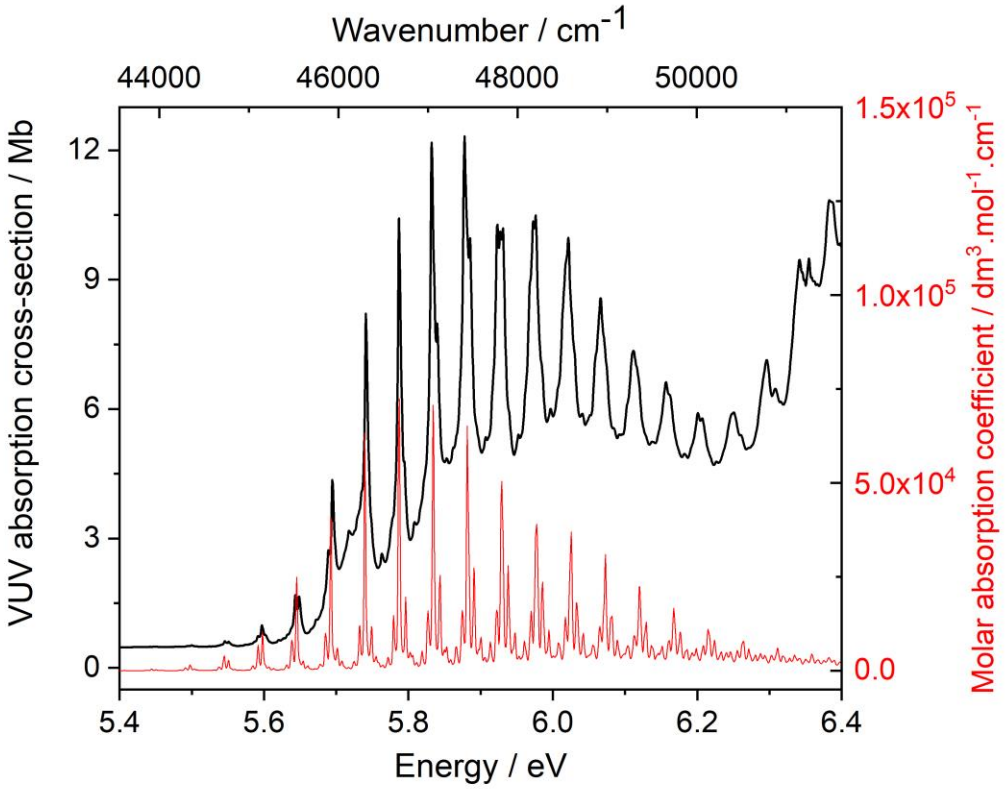

Variable temperature studies[26] suggested that the 0-0 band for the Rydberg state was 5.608 eV (45230 cm^{-1}). There is a direct correspondence between the most intense set of vibrations in the theoretical envelope, with frequency 360 cm^{-1}, and our calculated lowest a_1 mode 12 (381 cm^{-1}); the calculated values (MP2 was used here) are 5.8% high, were scaled to perform a complete fit. Weak bands attributed to the underlying $^1B_2$ state have no $^2B_1$ state counterpart, and this supports the $^1B_2$ assigned lines described above. The REMPI study of this Rydberg state by Xing et al[29] assigns a considerable number of line positions for both hot and cold bands. The principal cold band series identified by Xing et al, [29] was the main PES sequence 12_0^n where the quanta are n = 1 to 8; clearly this fits with both our PES analysis and the current Rydberg state study.

The principal focus of the Roos et al paper[30] was Rydberg states based on limiting ionic states $^2B_1$ and $^2A_1$; this included the observed $^1B_1$ $5b_13s$-state, and numerous higher Rydberg states. Their principal method was CASSCF, which was limited to the four π-orbitals discussed above, one from each irreducible representation, but were augmented for the Rydberg state studies.

Their work had a second level of approach based on multi-configurational second order perturbation theory method (the CASPT2 the PT2F variant). The latter gives very different VEE from the CASSCF values, and are much closer to experimental energy values. Our TDDFT corrected results are similar to those of Roos et al, [30] but NV_2 is low by about 0.1288 eV when compared with the EI results.

Rydberg states present very similar vibrational envelopes to that of the limiting ionic state for the series; our previous analysis[1] of the $^2B_1$ ionic state, shows a_1 modes, especially 4, 5, 7, 9 and 10, occur in binary combinations with mode 11. Some of these occur in up to quaternary combinations, and some in combination with even quanta of non-symmetric modes (e.g. $20a_2^2$). Herzberg-Teller calculations were performed, similar to those for the $^1A_2$ state above; the harmonic frequencies and labelling system used by G-09/G-16 is shown in the supplementary material at SM11. The most intense HT vibrations for the 1^1B_2 state, depicted in Table V, show that modes of all symmetries occur in the (total 1200) combination bands. However, the HT intensities are only ~1% when compared with the FC set.

7. NBD absorption in the 7.1 to 8.1 eV range. The NV_3 $^1B_1$ state.

The VUV envelope shows considerable changes in cross-section here, but with no simple pattern being evident. We assign this to the two highest valence states, NV_3 and NV_4, with underlying additional valence and/or Rydberg structure. Two calculated valence states for this region are the lowest 1^1B_1 with the 2^1B_2 state lying slightly higher in energy. NV_3 has two leading configurations in antisymmetric combination, but very unequal proportions, as follows:

0.690 $5b_1 8a_1^*$ (25 → 27) - 0.105 $5b_1 9a_1^*$ (25 → 30).

We assign the lower energy region to the 1^1B_1 state to a calculated origin at 6.856 eV (55295 cm^{-1}) with f(r) 0.0098, as shown in Figure 9; it shows an almost Gaussian set of bands which become more complex with number of vibrational satellites as the energy increases. We do not wish to imply that this calculated state is the sole participant in the 7.1 to 8.1 eV region. We

believe that (possibly several) other states lie under the envelope here. However, the *positions* of the calculated multiplet and the observed main peaks do give a relatively close correlation, and this is evidence for the assignment.

Table VI. Franck-Condon and Herzberg-Teller modes close to the origin and more intense combination bands for the $^1B_1$ state.

Position /cm^{-1}	Mode	FC intensity	HT intensity	Position /cm^{-1}	Mode	FC intensity	HT intensity
0	0-0	46	5	1105	2^1;1^1		44
363	1^1	275	16	1468	2^1;1^3		80
725	1^2	723	47	1831	2^1;1^4		93
1088	1^3	1785	76	2194	2^1;1^5		141
1451	1^4	2411	84	2556	2^1;1^6		112
1814	1^5	2258	112	3282	2^1;1^8		57
2177	1^6	2564	89	3318	7^1;1^7		17
2539	1^7	1742	53	1550	9^1;1^2		24
2902	1^8	891	42	2276	9^1;1^4		109
380	2^1	0	2	3463	9^1;1^5		71
779	7^1	12	0	3001	9^1;1^6		154
825	9^1	42	1	2293	9^1;2^3;1^3		70
860	11^1	0	3	2655	9^1;2^1;1^4		80
945	15^1	4	0	3018	9^1;2^1;1^5		127
970	16^1	0	1	1557	7^2	1	0
1078	20^1	0	3	1141	7^1;1^1	66	
1085	21^1	2	0	1504	7^1;1^2	249	
1288	27^1		1	1867	7^1;1^3	472	
1418	29^1		1	2210	2^2;1^4	14	
1586	31^1	22	1	2573	2^2;1^5	13	
3171	31^2	4	1	2986	3^2;1^6	41	
2706	33^1	2		2592	7^1;1^5	818	
2925	37^1	1		2955	7^1;1^6	688	
2993	38^1	2					

A summary of the principal vibrations are shown in Table VI. The $^1B_1$ state is dominated by the FC vibrations, while the fundamentals are dominated by the lowest a_1 frequency (mode 12, 363 cm^{-1}), but with low intensity. Not all of the a_1 fundamentals are active. Mode ($12a_1$) forms binary combinations with several other fundamentals including modes **11** (779), **10** (825), **8** (945), **7** (1085), **4**(1586), **3** (2706) **2** (2925) and **1** (2993 cm^{-1}). The binary combinations are generally 100 times more intense than the fundamentals. There is again significant Herzberg-Teller contributions, especially in the binary combinations. The HT bands occur in binary and

ternary combination bands. They have a simple effect of moving the centre of gravity of the combined set to slightly higher energy.

Figure 9. The 7.1 to 8.3 eV range with assignment of the $^1B_1$ state. Although the intensities of the local peaks vary erratically, their separation is more systematic, thereby enabling the $^1B_1$ state, which is dominated by groups of frequencies to be assigned. The line widths for for the theoretical spectrum, in red, is 10 cm^{-1}.

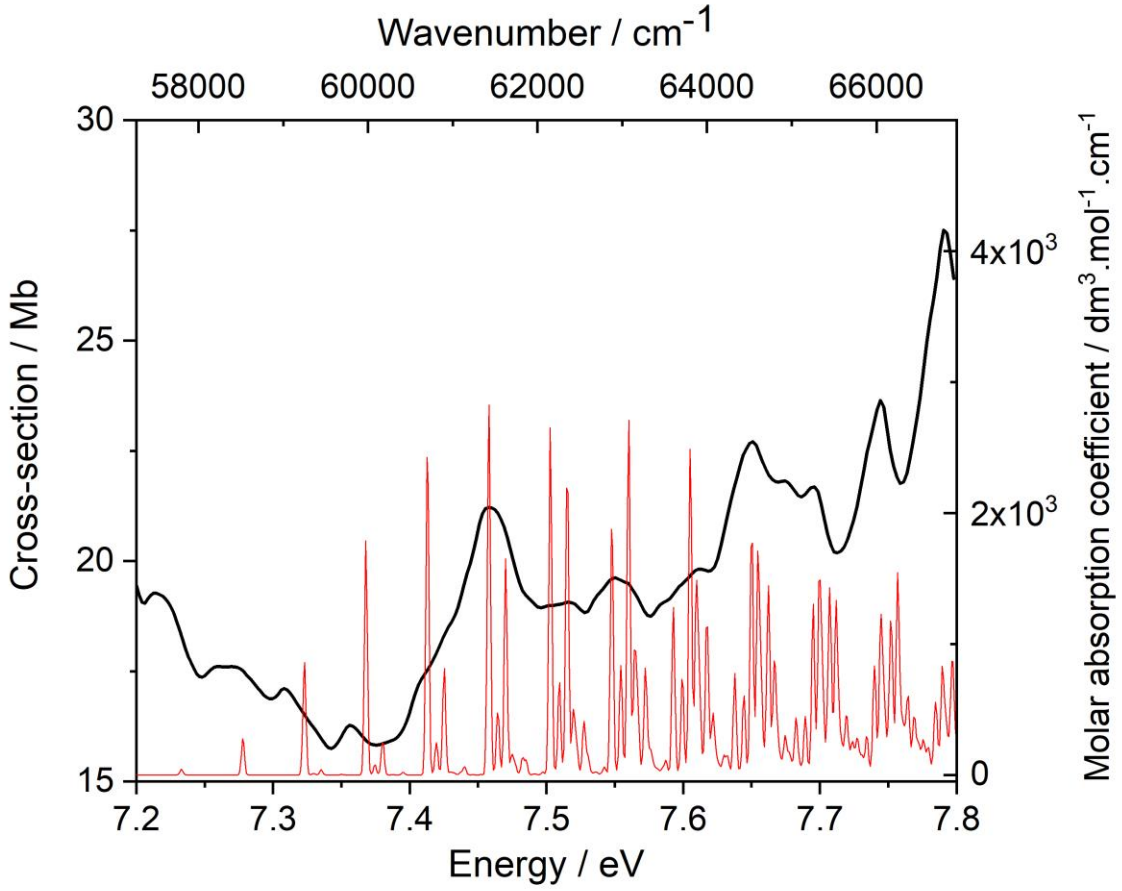

Figure 10. The NBD VUV spectrum from 7.7 to 8.4 eV with the Franck-Condon profile superimposed. Although many of the peaks have irregular intensity, they show spacing consistent with the 2^1B_2 calculated state. The full set of FC peaks shown are the summation of two separate sequences from two computations. Both used the same Half-Widths at Half-Maximum (HWHM) of 10 cm^{-1}. This leads to apparent disconuities in the curves in some places. As with other relatively high energy bands here, the observed spectrum and its fit is not expected to cover all the peaks observed. There is clearly a number of absorption bands in these regions of energy.

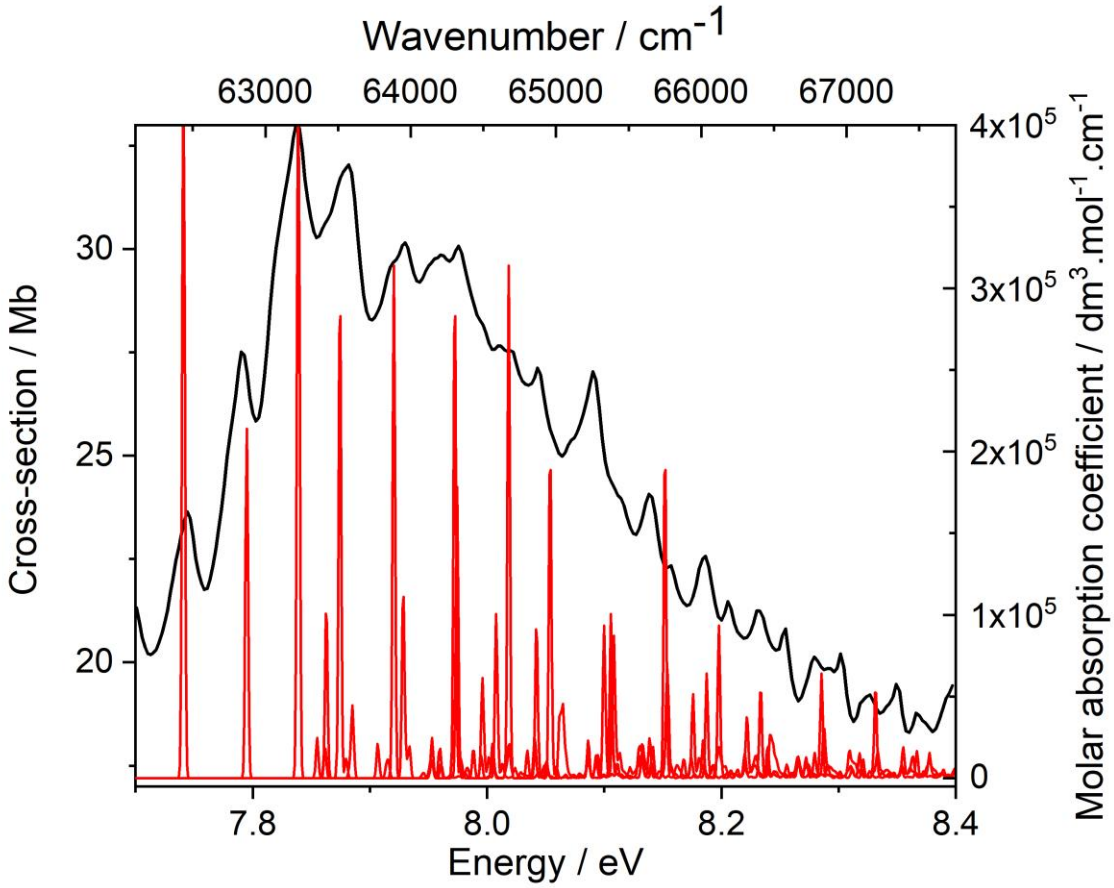

8. NBD absorption in the 7.1 to 8.1 eV range: the 2^1B_2 calculated state NV_4.

The 2^1B_2 calculated state, NV_4, has an even more complex wave-function, in contrast to that expected from the early analyses, as follows: 0.526 ($5b_13a_2$*) + 0.133 ($5b_14a_2$*) + 0.232 ($5a_15b_2$*) + 0.303 ($7a_15b_2$*).

This state, as with the 1^1B_2 state, shows the presence of an imaginary frequency under C_{2v} conditions; as previously, this is eliminated by projection with the largest overlap with a ground state frequency. The labelling for this process is shown in the supplementary material under SM11. The onset and a selection of the fundamentals together with the most intense higher frequency bands for the Franck-Condon and Herzberg-Teller modes are shown in Tables VII and VIII respectively. This band, shown in Figure 10, has a very complex envelope.

In the Franck-Condon vibrations, the 0-0 band is intense; the most prominent a_1 fundamentals in the Franck-Condon modes have sequence numbers 2, 7, 8, 9, 16, 21 and 28, with frequencies 346, 548, 709, 728, 920 and 1448 cm^{-1}.

Table VII B3LYP CIS 2^1B_2 state root 6 of the TDDFT sequence, with f(r) 0.1956, Franck-Condon profile. 0-0 band 7.031 eV

Position /cm^{-1}	*Excitation*	FC intensity	Position /cm^{-1}	*Excitation*	FC intensity
0	*0*	68260	1120	*21^1*	4855
192	*1^2*	10100	1122	*7^1;1^6*	444
346	*2^1*	75880	1154	*4^2;1^2*	463
383	*1^4*	3490	1168	*5^2;1^2*	426
538	*2^1;1^2*	17020	1172	*6^2;1^2*	281
548	*7^1*	15550	1231	*2^3;1^2*	1243
575	*1^6*	1337	1268	*2^2;1^6*	892
693	*2^2*	30740	1305	*2^1;1^10*	333
709	*8^1*	1586	1314	*7^1;1^8*	174
728	*9^1*	10230	1338	*27^1*	3883
730	*2^1;1^4*	5714	1345	*4^2;1^4*	156
739	*7^1;1^2*	3507	1359	*5^2;1^4*	149
767	*1^8*	537	1385	*2^4*	631
842	*3^2*	874	1419	*8^2*	133
884	*2^2;1^2*	6973	1422	*2^3;1^4*	427
901	*8^1;1^2*	361	1448	*28^1*	38450
920	*16^1*	123	1457	*9^2*	220
920	*9^1;1^2*	1472	1459	*2^2;1^8*	352
921	*2^1;1^6*	2128	1496	*2^1;1^12*	136
931	*7^1;1^4*	1185	1577	*2^4;1^2*	141
958	*1^10*	221	1614	*2^3;1^6*	163
962	*4^2*	2066	1643	*7^3*	158
976	*5^2*	1817	1651	*2^2;1^10*	143
981	*6^2*	1238	1651	*12^2*	508

The Herzberg-Teller vibrations for the 2^1B_2 state shown in Table VIII, are much more complex, and more vibrational states are shown in Table VIII to represent this situation. Most of the states contain b_2 modes, but all other symmetries are represented. Nearly 10000 vibrations containing up to 5 components were obtained; far more than for any other state studied. The sequence numbers in Table VIII also contain the symmetries of these contributors, and the mode sequence can be derived from the data given. The most intense fundamentals have b_2 symmetry; the most notable of these have frequencies 421, 759, 856 and 1053 cm^{-1}, but other

vibrational state symmetries also occur, such as 823, 1026 and 1202 cm^{-1} (a_2) and 1448 cm^{-1} (a_1). Generally, the binary and higher combinations occur at higher frequencies as expected, but their effect is to move the centre of gravity of the combined FC+HT bands to higher energy. The overall band is clearly more than 1 eV wide.

Table VIII B3LYP CIS 2^1B_2 state is root 6 of the TDDFT sequence, with f(r)=0.1956, Herzberg-Teller profile. The symmetries of the participating vibrations are indicated. The 0-0 band is at 7.031 eV

Position /cm^{-1}	*Excitation*	HT intensity	Position /cm^{-1}	*Excitation*	HT intensity
0	0	128	1510	22^1;2^1(b2+a1)	1474
346	2^1(a1)	208	1547	22^1;1^4(b2+4a2)	116
421	3^1(b2)	437	1548	13^1;2^2(b2+2a1)	180
442	2^1;1^1(a1+a2)	63	1654	26^1;2^1(b2+a1)	1964
693	2^2(2a1)	125	1690	26^1;1^4(b2+4a2)	149
759	10^1 (b2)	1093	1719	18^1;2^2(a2+2a1)	120
767	3^1;2^1(a1+b2)	415	1746	19^1;2^2(b2+2a2)	1516
823	11^1(a2)	59	1798	10^1;2^3(b2+3a1)	133
856	13^1(b2)	262	2129	20^1;19^1(a1+b2)	1501
951	10^1;1^2(b1+2a2)	251	2476	20^1;19^1;2^1(a1+b2+a1)	1541
1026	18^1(a2)	307	2501	28^1;19^1(a1+b2)	2163
1053	19^1(b2)	2487	2553	28^1;10^1;2^1(a1+b1+a1)	1532
1076	20^1(a1)	70	2612	28^1;22^1(a1+b2)	1315
1105	10^1;2^1(b1+a1)	1735	2730	26^1;20^1;2^1(b2+a1+a1)	1175
1113	3^1;2^2(b2+2a1)	264	2755	28^1;26^1(a1+b2)	1693
1164	22^1(b2)	1516	2847	28^1;19^1;2^1(a1+b2+a1)	2117
1202	23^1(a2)	188	2896	28^2(2a1)	356
1202	13^1;2^1(b2+a1)	438	2958	28^1;22^1;2^1(a1+b2+a1)	1322
1245	19^1;1^2(b2+2a2)	565	3086	32^1(b2)	752
1307	26^1(b2)	1957	3101	28^1;26^1;2^1(a1+b2+a1)	1756
1356	22^1;1^2(b2+2a2)	343	3146	36^1(b2)	929
1373	18^1;2^1(a2+a1)	317	3193	28^1;19^1;2^2(a1+b2+2a1)	1384
1399	19^1;2^1(b2+a1)	2355	3278	32^1;1^2(b2+2a2)	172
1436	19^1;1^4(b2+4a1)	192	3433	32^1;2^1(b2+a1)	1131
1448	28^1(a1)	354	3577	28^1;20^1;19^1(a1+a1+b2)	1221
1452	10^1;2^2(b2+2a1)	728	3924	28^1;20^1;19^1;2^1(a1+a1+b2+a1)	1295
1499	26^1;1^2(b2+2a2)	441	4343	28^3(3a1)	160

CONCLUSIONS

We have obtained the vacuum ultraviolet absorption spectra for norbornadiene. The spectrum shows a wide energy range where vibrational structure is present. A direct comparison of the earlier UV-absorption, REMPI spectrum and our VUV absorption, shown in Supplementary material SM3, demonstrates that our VUV absorption spectrum shows all the features observed

in the REMPI spectra, together with additional sub-structure. This is also present in the high-resolution photoelectron spectrum, but is not apparent in the REMPI spectra, and hence provides evidence of an underlying valence state, NV_2.

The deceptively simple analysis applied to the NBD UV absorption spectra by previous studies, is replaced by a more complex analysis, where many more $\sigma + \pi$ interactions occur. The TDDFT method is very successful in obtaining the equilibrium structure for a number of single excitation singlet and triplet states. The triplet state manifold was compared with electron impact spectra *en passant*, and that was the lead into detailed study of the singlet manifolds. Whilst the equilibrium structures for a number of singlet states were obtained with C_{2v} symmetry, it was found that several large basis sets showed a frequent preference for lower symmetry singlet states. This was attributed to relatively diffuse p-functions on the H-atoms, since omission of these led to the desired C_{2v} structures, with few saddle points occurring.

The Franck-Condon and Herzberg-Teller vibrational structure for several low-lying valence states was determined, and superimposed on the absorption spectrum. By choosing 'best fits' the calculated 0-0 band energies were corrected to estimates of the adiabatic excitation energies, for each of the NV_1 to NV_4 traditional valence states. For most states investigated, the HT intensities were only circa 10% of the FC ones. The presence of the $^1A_2$ state in the optical absorption spectrum is attributed to HT vibrations.

We have also obtained the VUV absorption spectrum of quadricyclane; it is fundamentally different with little vibrational structure, except that attributed to Rydberg states. The absence of a chromophore in QC is presumably responsible for this. Detailed analysis of the QC VUV spectrum is deferred, awaiting further experimental study.

SUPPLEMENTARY MATERIAL

See the supplementary material for additional information on each of the following:

1. The cleaned NBD and QC spectral onsets (Figures SM1a and SM1b). 2. Theoretical methods: additional material. 3. Comparison of details from the present VUV absorption

spectrum with previous UV and REMPI data. 4. The experimental photoelectron spectral onset of NBD with the theoretical Franck-Condon profile superimposed. 5. The mixing of p- and s-atomic orbitals (AOs) in NBD.6. Molecular structures for some singlet and triplet valence states of NBD.7. Excited state C-H bond structural changes.8. Electron impact variations.9. The a_1 frequencies for the $^3A_2$ and $^3B_2$ states.10. Adiabatic excitation energies (AEE) and oscillator strengths at the TDDFT level.11. The harmonic frequencies for the excited states.12. The 7.5 to 8.5 eV region: a potential alternative assignment.13. Extended list of singlet state energies using the TDDFT method.

ACKNOWLEDGEMENTS

We thank: (a) the ASTRID2 Synchrotron facility, and Aarhus University, for a grant of beam-time; (b) the Italian MIUR (under the project PON01-010788); (c) the University of Edinburgh (Eddie3) and Edinburgh Parallel Computing Centre (Cirrus) super-computing facilities for support.

DATA AVAILABILITY OF ARTICLE OR SUPPLEMENTARY MATERIAL.

The data that support the findings of this study, including its supplementary material, will be available from the corresponding author upon reasonable request.

REFERENCES

1. M. H. Palmer, M. Coreno, M. de Simone, C. Grazioli, R. A. Aitken, S. Vrønning Hoffmann, N. C. Jones and C. Peureux, *J. Chem. Phys*. **153**, 204303 (2020). https://doi.org/10.1063/5.0031387
2. M. H. Palmer, S. Vrønning Hoffmann, N. C. Jones, M. Coreno, M. de Simone, C. Grazioli, and R. A. Aitken, *J. Chem. Phys.* **153**, 054301 (2020). https://doi.org/10.1063/5.0011088
3. M. H. Palmer, R. A. Aitken, M. Coreno, M. de Simone, C. Grazioli, S. Vrønning Hoffmann, and N. C. Jones, *J. Chem. Phys.* **152**, 144301 (2020). https://doi.org/10.1063/1.5142268
4. U. Bauer, L. Fromm, C. Weiß, P. Bachmann, F. Späth, F. Düll, J. Steinhauer, W. Hieringer, A. Görling, A. Hirsch, H.-P. Steinrück, and C. Papp, *J. Phys. Chem. C* **123**, 7654–7664 (2019). https://doi.org/10.1021/acs.jpcc.8b03746
5. U. Bauer, L. Fromm, C. Weiß, F. Späth, P. Bachmann, F. Düll, J. Steinhauer, S. Matysik, A. Pominov, A. Görling, A. Hirsch, H.-P. Steinrück, and C. Papp, *J. Chem. Phys.* **150**, 184706 (2019). https://doi.org/10.1063/1.5095583
6. O. Brummel, F. Waidhas, U. Bauer, Y. Wu, S. Bochmann, H-P. Steinrück, C. Papp, J. Bachmann, and J. Libuda, *J. Phys. Chem. Lett.* **8**, 2819–2825 (2017). https://doi.org/10.1021/acs.jpclett.7b00995
7. A. Valentini, S. van den Wildenberg and F. Remacle, *Phys. Chem. Chem. Phys*., **22**, 22302–22313 (2020). https://doi.org/10.1039/D0CP03435E
8. B. E. Tebikachew, H. B. Li, A. Pirrotta, K. Borjesson, G. C. Solomon, J. Hihath, and K. Moth-Poulsen, *J. Phys. Chem. C* **121**, 7094–7100 (2017).
https://doi.org/10.1021/acs.jpcc.7b00319
9. B. E. Tebikachew, F.Edhborg, N. Kann, B. Albinsson, and K. Moth-Poulsen, *Phys. Chem. Chem. Phys.* **20**, 23195–23201 (2018). https://doi.org/10.1039/C8CP04329A
10. M. Quant, A. Lennartson, A. Dreos, M. Kuisma, P. Erhart, K. Börjesson, and K. Moth-Poulsen, *Chem. Eur. J.* **22**, 13265–13274 (2016). https://doi.org/10.1002/chem.201602530

11. A. Cuppoletti, J. P. Dinnocenzo, J. L. Goodman, and I. R. Gould, *J. Phys. Chem. A* **103**, 11253–11256 (1999). https://doi.org/10.1021/jp992884i
12. M. Bertram, F. Waidhas, M. Jevric, L. Fromm, C. Schuschke, M. Kastenmeier, A. Görling, K. Moth-Poulsen, O. Brummel, and J. Libuda, *J. Chem. Phys.* **152**, 044708 (2020). https://doi.org/10.1063/1.5137897
13. A. Dreos, Z. Wang, B. E. Tebikachew, K. Moth-Poulsen, and J. Andreasson, *J. Phys. Chem. Lett.* **9**, 6174–6178 (2018). https://doi.org/10.1021/acs.jpclett.8b02567
14. M. Quant, A. Hamrin, A. Lennartson, P. Erhart, and K. Moth-Poulsen, *J. Phys. Chem. C* **123**, 7081–7087 (2019). https://doi.org/10.1021/acs.jpcc.9b02111
15. J. Gębicki , S. Kuberski, and R. Kamiński, *J. Phys. Org. Chem*. **2**, 383–388 (1989). https://doi.org/10.1002/poc.610020504
16. (a) M. B. Robin, 'Higher Excited States of Polyatomic Molecules', Volume II, Chapter V, p176-180, Academic Press, New York, (1975). (b) M. B. Robin, 'Higher Excited States of Polyatomic Molecules', Volume III, Chapter XVII, p329-332, Academic Press, New York, (1985)
17. B. C. Roquitte, *J. Phys. Chem.* **69**, 2475–2477 (1965). https://doi.org/10.1021/j100891a509
18. M. H. Palmer, M. Coreno, M. de Simone, C. Grazioli, S. Vrønning Hoffmann, and N. C. Jones, *J. Chem. Phys*. **150**, 194305 (2019). https://doi.org/10.1063/1.5096254
19. M. H. Palmer, S. Vrønning Hoffmann, N. C. Jones, M. Coreno, M. de Simone, and C. Grazioli, *J. Chem. Phys.* **151**, 084304 (2019). https://doi.org/10.1063/1.5115997
20. R. Hoffmann, A. Imamura, and W. J. Hehre, *J. Am. Chem. Soc.* **90**, 1499–1509 (1968). https://doi.org/10.1021/ja01008a018
21. R. Hoffmann, E. Heilbronner, and R. Gleiter, *J. Am. Chem. Soc.* **92**, 706–707 (1970). https://doi.org/10.1021/ja00706a051
22. R. Hoffmann, *Acc. Chem. Res.* **4**, 1–9 (1971). https://doi.org/10.1021/ar50037a001
23. R. S. Mulliken, *J. Chem. Phys.* **7**, 20–34 (1939). https://doi.org/10.1063/1.1750319
24. C. F. Wilcox, S. Winstein and W. G. McMillan, *J. Am. Chem. Soc.* **82**, 5450–5454 (1960). https://doi.org/10.1021/ja01505a037
25. N. L. Allinger and M. A. Miller, *J. Am. Chem. Soc.* **86**, 2811–2819 (1964). https://doi.org/10.1021/ja01068a012
26. M. B. Robin and N. A. Kuebler, *J. Chem. Phys.* **44**, 2664–2671 (1966). https://doi.org/10.1063/1.1727108
27. M. B. Robin and N. A. Kuebler, *J. Mol. Spectrosc.* **33**, 274–291 (1970). https://doi.org/10.1016/0022-2852(70)90039-1
28. J. P. Doering and R. McDiarmid, *J. Chem. Phys.* **75**, 87–91 (1981) https://doi.org/10.1063/1.441858
29. X. Xing, A. Gedanken, A-H. Sheybani and R. McDiarmid, *J. Phys. Chem.* **98**, 8302–8309 (1994). https://doi.org/10.1021/j100085a007
30. B. O. Roos, M. Merchan, R. McDiarmid, and X. Xing, *J. Am. Chem. Soc.* **116**, 5927–5936 (1994). https://doi.org/10.1021/ja00092a049
31. R. P. Frueholz, W. M. Flicker, O. A. Mosher, and A. Kuppermann, J. Chem. Phys. **70**, 1986–1993 (1979). https://doi.org/10.1063/1437624
32. M. Allan, *J. Electron Spectrosc. Relat. Phenom.* **48**, 219–351 (1989). https://doi.org/10.1016/0368-2048(89)80018-0
33. M. H. Palmer, T. Ridley, S. Vrønning Hoffmann, N. C. Jones, M. Coreno, M. de Simone, C. Grazioli, M. Biczysko, A. Baiardi, and P. Limão-Vieira, J. Chem. Phys. **142**, 134302 (2015). https://doi.org/10.1063/1.4916121
34. Gaussian 16 Revision A.03 M. J. Frisch G. W. Trucks H. B. Schlegel G. E. Scuseria M. A. Robb J. R. Cheeseman G. Scalmani V. Barone G. A. Petersson H. Nakatsuji X. Li M. Caricato A. V. Marenich J. Bloino B. G. Janesko R. Gomperts B. Mennucci H. P. Hratchian J. V. Ortiz

A. F. Izmaylov J. L. Sonnenberg D. Williams-Young F. Ding F. Lipparini F. Egidi J. Goings B. Peng A. Petrone T. Henderson D. Ranasinghe V. G. Zakrzewski J. Gao N. Rega G. Zheng W. Liang M. Hada M. Ehara K. Toyota R. Fukuda J. Hasegawa M. Ishida T. Nakajima Y. Honda O. Kitao H. Nakai T. Vreven K. Throssell J. A. Montgomery Jr. J. E. Peralta F. Ogliaro M. J. Bearpark J. J. Heyd E. N. Brothers K. N. Kudin V. N. Staroverov T. A. Keith R. Kobayashi J. Normand K. Raghavachari A. P. Rendell J. C. Burant S. S. Iyengar J. Tomasi M. Cossi J. M. Millam M. Klene C. Adamo R. Cammi J. W. Ochterski R. L. Martin K. Morokuma O. Farkas J. B. Foresman and D. J. Fox Gaussian Inc. Wallingford CT 2016.
35. R. J. Buenker and S. Krebs, in Recent Advances in Computational Chemistry (1999), **4** (Recent Advances in Multireference Methods), 1-29. The configuration-driven approach for multireference configuration interaction calculations.
36. M. F. Guest, I. J. Bush, H. J. J. Van Dam, P. Sherwood, J. M. H. Thomas, J. H. Van Lenthe, R. W. A. Havenith, and J. Kendrick, *Mol. Phys.* **103**, 719–747 (2005). https://doi.org/10.1080/00268970512331340592
37. V. Barone, J. Bloino, M. Biczysko, and F. Santoro, *J. Chem. Theory Comput.* **5**, 540–554 (2009). https://doi.org/10.1021/ct8004744
38. J. Bloino, M. Biczysko, F. Santoro, and V. Barone, *J. Chem. Theory Comput.* **6**, 1256–1274 (2010). https://doi.org/10.1021/ct9006772
39. A. Baiardi, J. Bloino, and V. Barone, *J. Chem. Theory Comput.* **9**, 4097–4115 (2013). https://doi.org/10.1021/ct400450k
40. P. Hohenberg and W. Kohn, *Phys. Rev.* **136,** B864–B871 (1964). https:doi.org/10.1103/PhysRev.136.B864
41. W. Kohn and L. J. Sham, *Phys. Rev.* **140**, A1133–A1138 (1965). https://doi.org/10.1103/PhysRev.140.A1133
42. R. G. Parr and W. Yang, '*Density-functional theory of atoms and molecules'*, Oxford University Press, Oxford, 1989.
43. A. D. Becke, *J. Chem. Phys.* **98**, 5648–5652 (1993). https://doi.org/10.1063/1.464913
44. T. Yanai, D. Tew, and N. Handy, *Chem. Phys. Lett.* **393**, 51–57 (2004). https://doi.org/10.1016/j.cplett.2004.06.011
45. R. Ahlrichs and P. R. Taylor, *J. Chim. Phys.* **78**, 315–324 (1981). https://doi.org/10.1051/jcp/1981780315
46. A. Schaefer, H. Horn, and R. Ahlrichs, *J. Chem. Phys.* **97**, 2571–2577 (1992). https:doi/org/10.1063/1.463096
47. A. Schaefer, C. Huber, and R. Ahlrichs, *J. Chem. Phys.* **100**, 5829–5835 (1994). https://doi.org/10.1063/1.467146
48. B. P. Pritchard, D. Altarawy, B. Didier, T. D. Gibson, T. L. Windus, *J. Chem. Inf. Model.* **59**, 4814–4820 (2019). https://doi.org/10.1021/acs.jcim.9b00725.
49. D. A. Lightner, J. K. Gawronski, T. D. Bouman, *J. Am. Chem. Soc.* **102**, 5749–5754 (1980). https://doi.org/10.1021/ja00538a009
50. R. B. Hermann, *J. Org. Chem.* **27**, 441–442 (1962). https://doi.org/10.1021/jo01049a023
51. M. H. Palmer, *J. Mol. Struct.* **161**, 333–345 (1987). https://doi.org/10.1016/0022-2860(87)85085-8
52. M. H. Palmer and R. H. Findlay, *Chem. Phys. Lett.* **15**, 416–420 (1972). https://doi.org/10.1016/0009-2614(72)80204-5
53. M. K. Zgierski and F. Zerbetto, *J. Chem. Phys.* **98**, 14–20 (1993). https://doi.org/ doi/10.1063/1.464664
54. A. Yokozeki and K. Kuchitsu, *Bull. Chem. Soc. Jpn.* **44**, 2356–2363 (1971). https://doi.org/10.1246/bcsj.44.2356
55. G. Knuchel, G. Grassi, B. Vogelsanger, and A. Bauder, *J. Am. Chem. Soc.* **115**, 10845–10848 (1993). https://doi.org/10.1021/ja00076a047

Palmer et al Fig.1

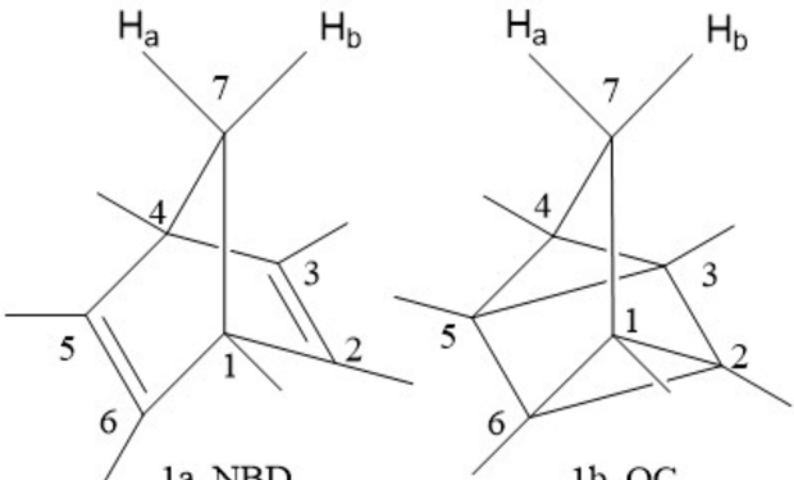

Palmer et al Figure 2

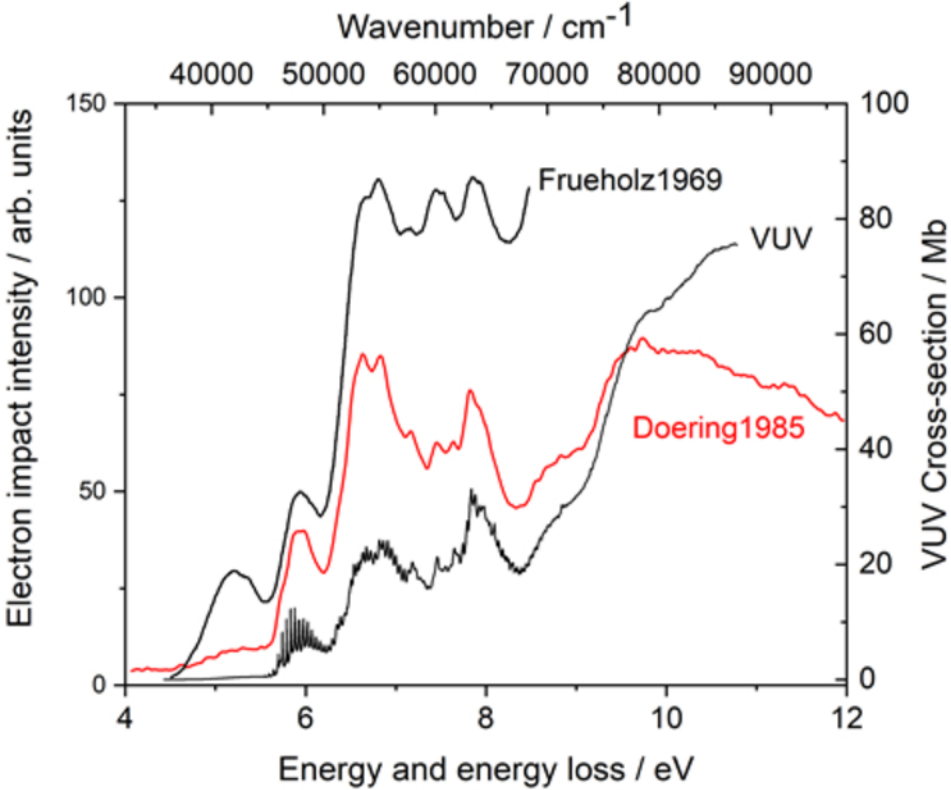

Palmer et al, Fig.3

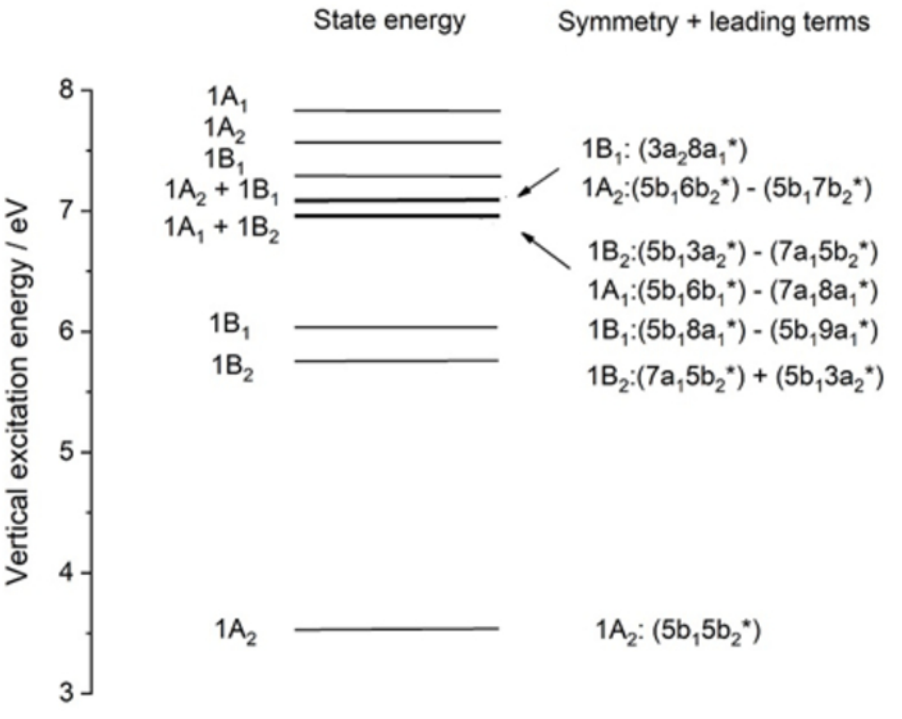

Palmer et al, Fig.5

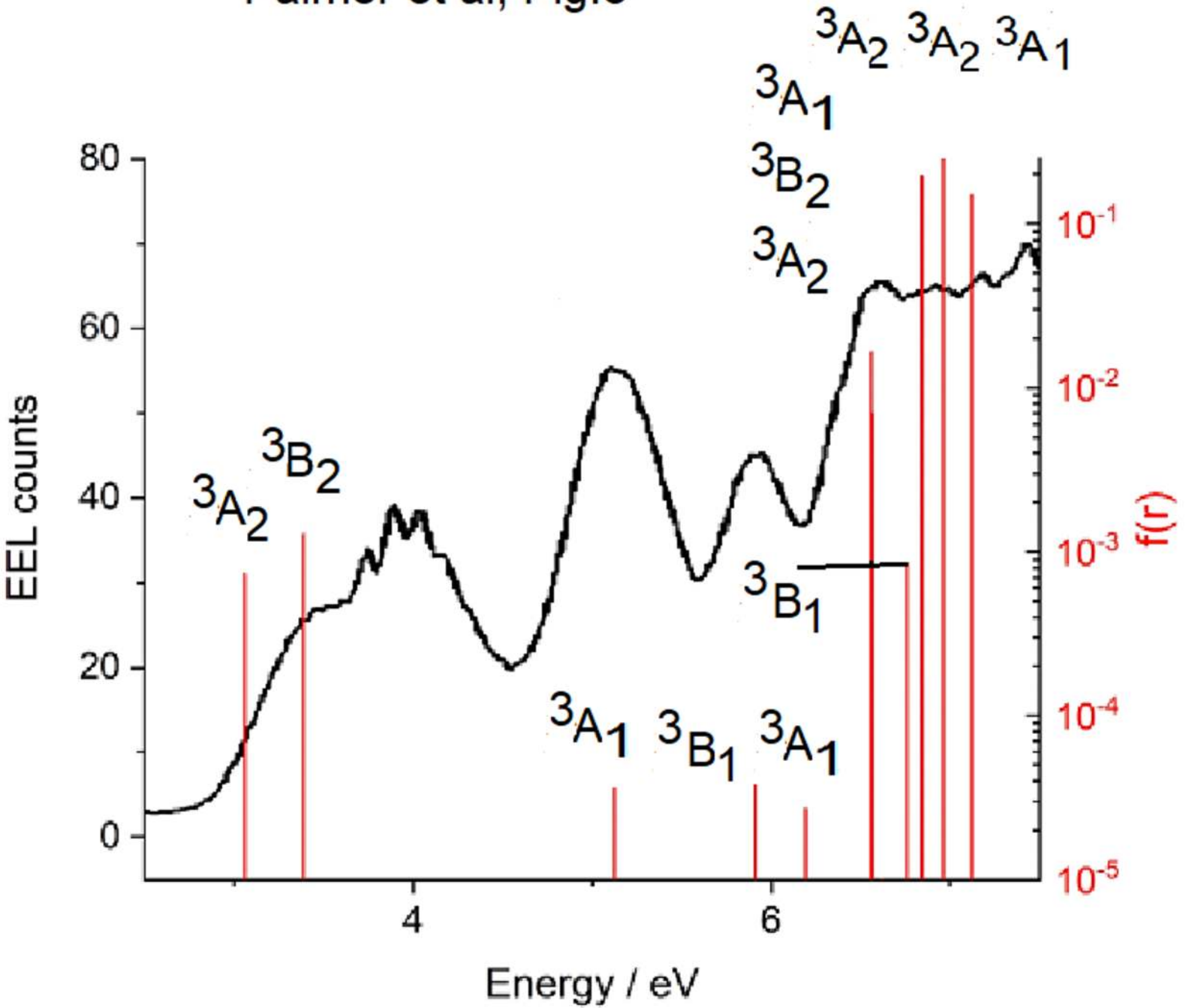

Palmer et al, Fig. 5

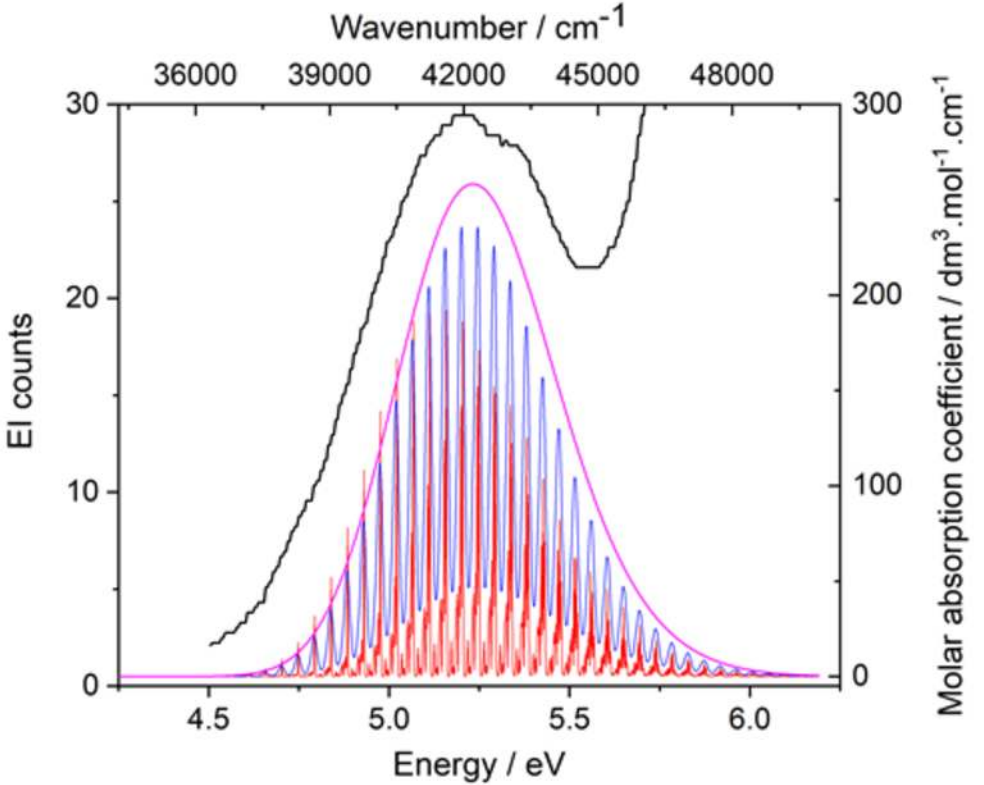

Palmer et al, Fig. 6

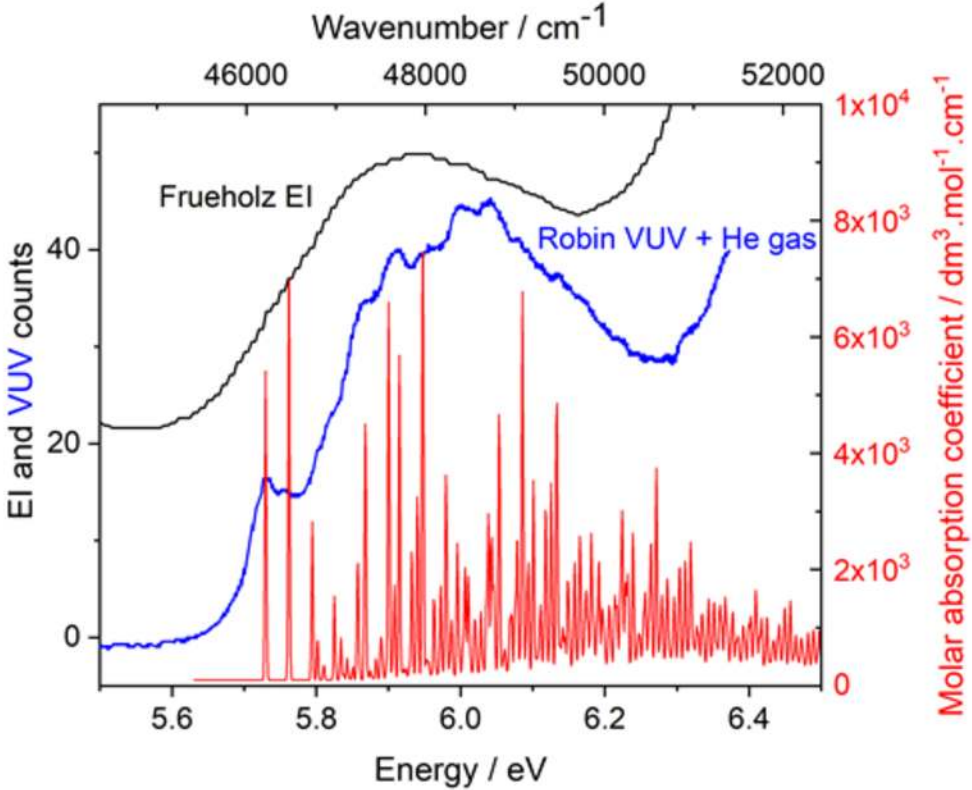

Palmer et al Fig. 7

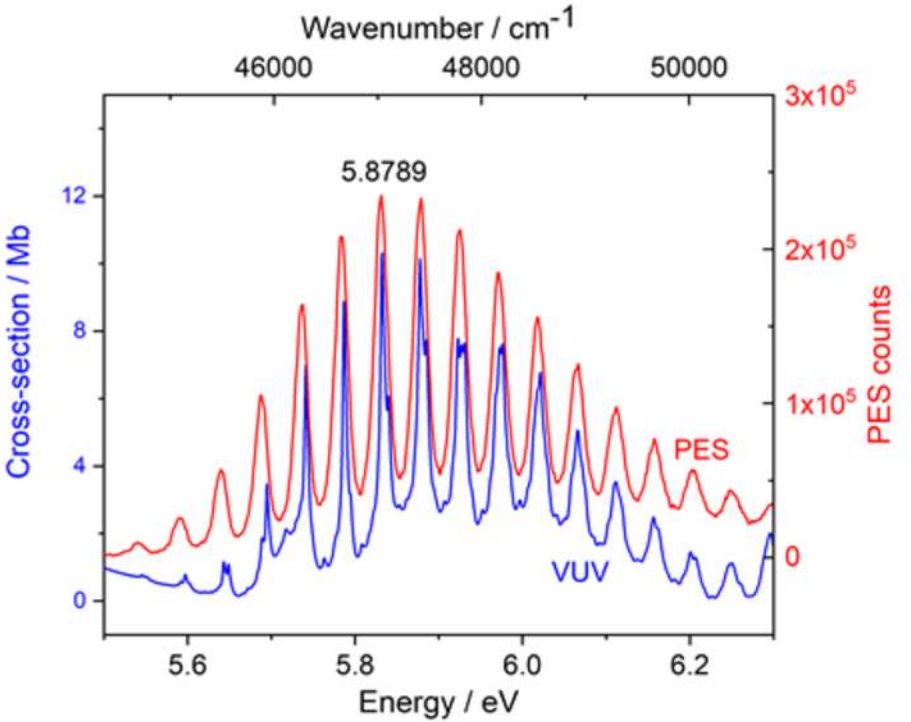

Palmer et al Fig. 8

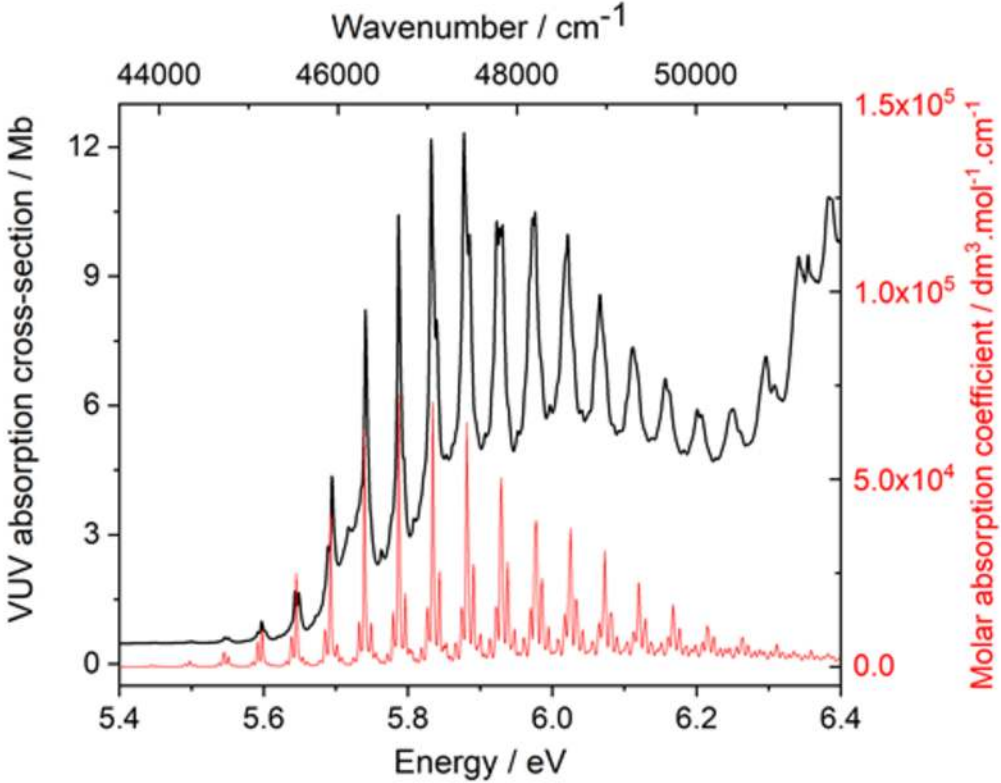

Palmer et al Figure 9

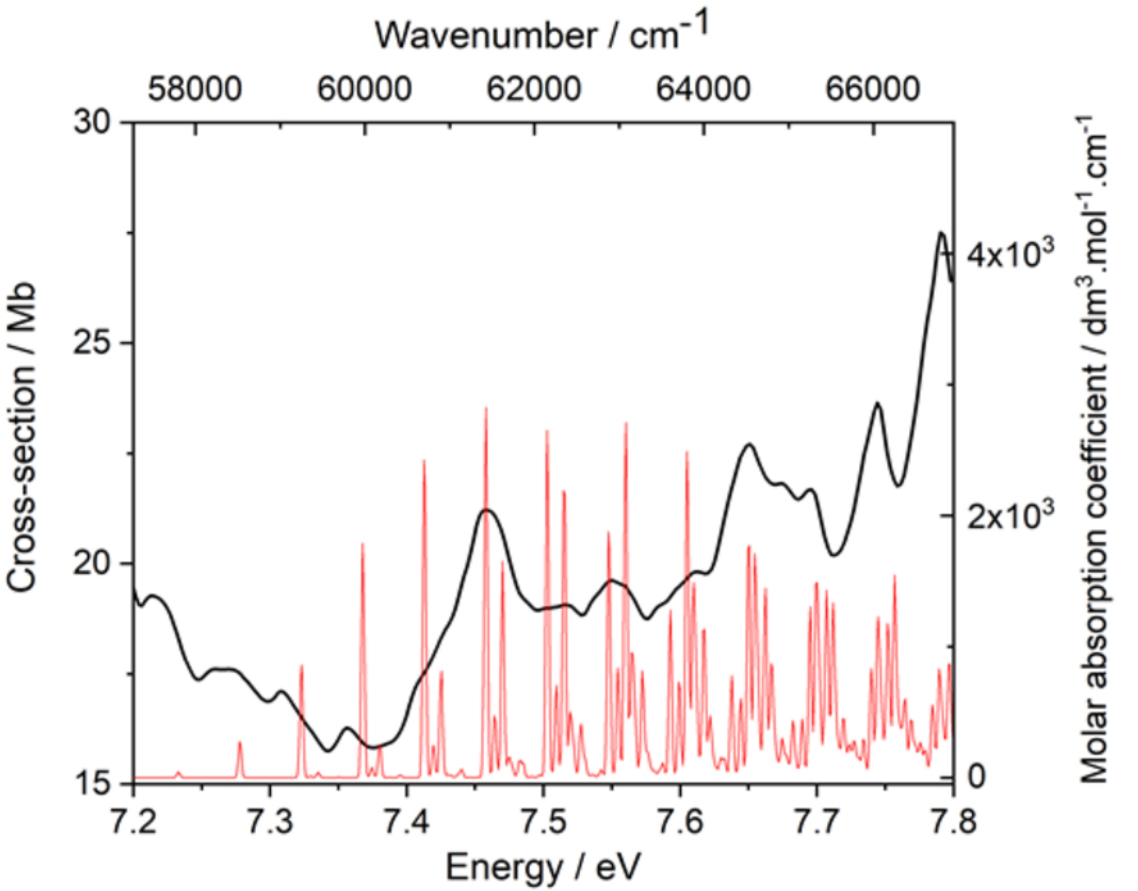

Palmer et al Figure 10